

FRACTIONAL DIFFUSION ON GRAPHS: SUPERPOSITION OF LAPLACIAN SEMIGROUPS AND MEMORY

NIKITA DENISKIN AND ERNESTO ESTRADA*

ABSTRACT. Subdiffusion on graphs is often modeled by time-fractional diffusion equations, yet its structural and dynamical consequences remain unclear. We show that subdiffusive transport on graphs is a memory-driven process generated by a random time change that compresses operational time, produces long-tailed waiting times, and breaks Markovianity while preserving linearity and mass conservation. We prove that Mittag-Leffler graph dynamics admit an exact convex, mass-preserving representation as a superposition of classical heat semigroups evaluated at rescaled times, revealing fractional diffusion as ordinary diffusion acting across multiple intrinsic time scales. This framework uncovers heterogeneous, vertex-dependent memory effects and induces transport biases absent in classical diffusion, including algebraic relaxation, degree-dependent waiting times, and early-time asymmetries between sources and neighbors. These features define a subdiffusive geometry on graphs enabling particles to locally discover global shortest paths while favoring high-degree regions. Finally, we show that time-fractional diffusion arises as a singular limit of multi-rate diffusion.

MSC: 26A33; 15A16; 35R11; 47D06; 45D05

Keywords: Subdiffusion on graphs; Time-fractional diffusion; Mittag-Leffler functions; Memory kernels; Sum-of-exponentials; Shortest paths

CONTENTS

1. Introduction	2
1.1. Subdiffusion: physical mechanisms and mathematical models	4
1.2. Contributions of the paper	6
2. Preliminaries	7
2.1. Notation and assumptions	7
2.2. Subordination identity and the M–Wright density	7
2.3. Complete monotonicity and Bernstein’s theorem.	8
2.4. Terminology: subordination and the random clock	8
2.5. The time–changed process X_{E_t}	9
3. Sum of Exponentials approximation	9
3.1. SOE via log–trapezoidal quadrature	10
3.2. SOE discretization via subordination: quadrature weights, mass preservation, and vertex survivals	11
4. Tail bounds for the subordination integral and window selection	12
4.1. Left tail (small θ)	12
4.2. Right tail (large θ)	12
4.3. Putting it together: window rules	13
4.4. Constants in the stretched-exponential bound.	13
5. Vertex waiting times and error metrics.	14

5.1.	Raw vs. normalized quadrature weights.	14
5.2.	Mixture interpretation for the random clock.	14
5.3.	Error metrics	15
5.4.	Computational results	16
6.	Subdiffusive distance and paths	17
6.1.	Subdiffusive distance	17
6.2.	Subdiffusive shortest paths	18
6.3.	Subdiffusive shortest paths on a geometric graph	21
7.	Caputo fractional derivative and memory	25
7.1.	Physical Interpretation: Memory Regimes on a Graph	29
8.	How memory emerges from fractional diffusion on a graph?	30
8.1.	Local Convexity and Concavity in Caputo Fractional Diffusion: A Mittag-Leffler and SOE-Based Analysis	30
8.2.	Random time change induces subdiffusion and memory	32
9.	A generalized physico-mathematical context of subdiffusion on graphs	33
9.1.	A multiplex diffusion	33
9.2.	Factorized high-order temporal diffusion equation	34
9.3.	Operator-valued memory and diffusion on graphs	36
	Conclusions	41
10.	Appendix	42
	References	44

1. INTRODUCTION

Graphs $G = (V, E)$ —also referred to as networks—provide a natural mathematical framework to represent a wide variety of complex systems arising in molecular, ecological, technological, and social contexts [16]. In this representation, the set of vertices V typically corresponds to the entities of the system, while the set of edges E encodes their interactions. A fundamental mechanism governing the transport of mass, energy, or information across such networks is diffusion [41, 47]. However, due to the complexity of the environments in which many real-world networks are embedded, transport processes often deviate from classical diffusive behavior [53, 52, 64, 48].

Subdiffusion, characterized by a slower-than-linear growth of the mean squared displacement, is especially prevalent in complex systems. For instance, subdiffusive dynamics are ubiquitous in the crowded interior of biological cells [71, 28, 27, 4], where millions of macromolecules interact, forming intricate networks of biochemical processes. Similarly, crowding effects caused by vehicle density and driving fluctuations in urban transportation systems have been shown to induce subdiffusive traffic states [13]. Subdiffusion has also been observed in information transmission processes on online social networks, such as Twitter (now X) and Digg [21].

A standard mathematical approach to model such crowded and heterogeneous systems is to replace the classical time derivative in the diffusion equation with a fractional-time derivative [19, 65]. When anomalous diffusion takes place on a

graph G , this leads to the following fractional diffusion equation:

$$(1.1) \quad \begin{cases} D_t^\alpha u_\theta(t) + \theta L u_\theta(t) = 0, \\ u_\theta(0) = u_0, \end{cases}$$

where $\theta > 0$ denotes the diffusivity and L is the graph Laplacian operator acting on functions defined on the vertex set. Specifically, L is the linear mapping from $\mathbb{C}(V)$ into itself given by

$$(1.2) \quad (Lf)(v) := \sum_{(v,w) \in E} (f(v) - f(w)), \quad f \in \mathbb{C}(V),$$

which is known as the graph Laplacian. The operator D_t^α denotes the Caputo time-fractional derivative of order $0 < \alpha < 1$ [9], defined by

$$(1.3) \quad D_t^\alpha u(t) = \frac{1}{\Gamma(1-\alpha)} \int_0^t \frac{u'(\tau)}{(t-\tau)^\alpha} d\tau,$$

where $u'(\tau)$ is the first derivative of u evaluated at time τ . Despite their broad relevance in continuous settings, time-fractional diffusion models have been only sparsely explored on graphs and networks. To date, applications have been largely restricted to epidemiological modeling [1, 14] and to the fractional diffusion on the human proteome, proposed as an alternative framework to account for the multi-organ damage associated with SARS-CoV-2 infection [17]. An exception is the use of (1.1) in an engineering context for searching consensus of autonomous systems, where it receive the name of “fractional order consensus” [67, 72, 66, 31, 42, 8]. A rapidly growing line of research explores the integration of fractional derivatives into learning algorithms, leading to the development of fractional-order neural networks and related architectures, with emerging applications in machine learning and artificial intelligence [55, 32].

Apart from crowding and excluded-volume effects, which reduce mobility by limiting the available space for motion, several additional mechanisms can give rise to subdiffusion in complex systems. This happen, for instance in ecological networks, where structural disorder and heterogeneity—manifested through irregular geometries, bottlenecks, and hierarchical or fractal structures—constrain transport pathways and significantly slow down spatial exploration [35]. These features often induce trapping events and lead to broad distributions of residence times. Another characteristic of complex systems is the existence of memory. Temporal memory effects have been observed, for instance, in transcription regulator–DNA interactions in live bacterial cells [33], apart from the large existing evidence accumulated on single-cell experiments. As memory refers to the phenomenon where past events influence a system’s current and future states or behaviors, the evolution of these complex systems at a given time depends on its entire past history rather than solely on its instantaneous state.

In such non-Markovian settings, classical diffusion equations fail to provide an adequate description. Instead, diffusion models with memory kernels naturally arise, capturing the nonlocal-in-time response induced by trapping, heterogeneity, and temporal correlations [59, 29, 57, 58, 70, 68]. Once again, in the case of graphs, this leads to the generalized diffusion equation

$$(1.4) \quad \begin{cases} \int_0^t \gamma(t-s) \partial_s u_\theta(s) ds + \theta L u_\theta(t) = 0, \\ u_\theta(0) = u_0, \end{cases}$$

where $\gamma(t)$ denotes a memory kernel. Such formulations provide a unifying framework for describing subdiffusive transport and establish a direct connection between microscopic mechanisms and macroscopic anomalous diffusion. Related non-Markovian formulations on networks arise naturally when vertex-to-vertex motion is modeled as a non-Poisson continuous-time random walk. In this setting, the node-state evolution is governed by a generalized master equation in which the graph Laplacian (or transition operator) appears entwined in time with a kernel determined by the waiting-time distribution, and memory effects are known to substantially alter diffusion and mixing properties on (temporal) networks [30, 38, 62].

While time-fractional diffusion equations and memory-kernel formulations are widely used to model subdiffusive transport in continuous settings, their role in the context of networks and graph-based diffusion has so far been explored mainly at a phenomenological level. Existing studies typically emphasize anomalous scaling, spectral properties, or long-time relaxation, but often treat memory as a uniform slowing-down mechanism acting on otherwise classical graph diffusion [37, 34, 22]. As a result, comparatively little is known about how non-Markovian effects interact with the discrete geometry of a graph, how they influence transport pathways, or how they modify vertex-level and path-level behavior beyond global decay rates.

The present work is motivated by the need to clarify how subdiffusion reshapes diffusion on graphs at the structural level. By exploiting the subordination principle and a mass-preserving sum-of-exponentials representation of the Mittag-Leffler operator, we connect fractional diffusion on graphs to superposition of classical heat processes acting at different internal times. This perspective allows us to study, in a unified way, memory effects, vertex-dependent waiting times, effective distances, and path selection in subdiffusive dynamics. In doing so, we show that memory does not merely slow down diffusion uniformly, but induces heterogeneous temporal behavior across vertices and leads to well-defined subdiffusive distances and paths that differ from their classical diffusive counterparts. These results provide a concrete link between fractional models, memory kernels, and graph-based transport, and offer a more detailed understanding of what subdiffusion means when the underlying space is a network.

1.1. Subdiffusion: physical mechanisms and mathematical models. A central hallmark of anomalous diffusion is the deviation of the mean squared displacement (MSD) from the linear-in-time growth predicted by Fickian diffusion. Instead, one observes a power-law scaling [64, 6, 52]

$$(1.5) \quad \langle x^2(t) \rangle \sim t^\alpha, \quad 0 < \alpha < 1,$$

which defines subdiffusive behavior. As emphasized in [64], such subdiffusion is not a single phenomenon but rather a collective outcome of different physical mechanisms, each leading to distinct stochastic and mathematical descriptions.

One prominent mechanism underlying subdiffusion is trapping [65, 64, 19]. In crowded or energetically disordered environments, particles may experience long waiting times between successive displacements due to transient binding or deep

potential wells. This situation is naturally described by the continuous-time random walk (CTRW) framework, where the waiting times between steps are independent random variables drawn from a heavy-tailed distribution

$$(1.6) \quad \psi(\tau) \sim \tau^{-1-\alpha}, \quad 0 < \alpha < 1,$$

implying a diverging mean waiting time.

In the scaling limit, CTRW dynamics lead to a fractional diffusion equation (FDE) for the probability density $p(x, t)$. Sokolov [64] stresses that the use of such fractional equations is physically justified only when the underlying trapping assumptions are valid. CTRW models generally exhibit aging, weak ergodicity breaking, and large trajectory-to-trajectory fluctuations.

Another class of subdiffusive systems arises from transport in labyrinthine or fractal structures, such as percolation clusters or tortuous channel networks [56, 64, 51, 20]. In these systems, anomalous diffusion originates from geometric constraints rather than trapping times. The particle explores a space with no translational invariance and a broad distribution of path lengths.

A paradigmatic example is diffusion on critical percolation clusters or related fractal media, for which the MSD again follows a subdiffusive power law. While fractional diffusion equations may reproduce the probability density in unbounded domains, Sokolov [64] emphasizes that they generally fail to capture important properties such as first-passage times or confined-domain behavior. Consequently, geometric subdiffusion and trapping-induced subdiffusion can yield identical PDFs while corresponding to fundamentally different physical processes.

Subdiffusion may also emerge in viscoelastic environments [25, 10, 26], where the tagged particle is embedded in a complex interacting medium, such as a polymer network or the cytoskeleton. In this case, the dynamics is not governed by trapping or geometry but by long-range temporal correlations in the particle's motion.

These systems are often described by fractional Brownian motion (fBm), a Gaussian process characterized by correlated increments, or equivalently by generalized Langevin equations (GLEs) with memory kernels,

$$(1.7) \quad m\dot{v}(t) = - \int_0^t G(t-t') v(t') dt' + \xi(t),$$

where the friction kernel typically follows a power law $G(t) \sim t^{-\beta}$, and $\xi(t)$ is a correlated noise term. Depending on the noise properties, the resulting MSD scales subdiffusively. Unlike CTRW-based models, fBm and GLE dynamics are ergodic and do not exhibit aging, a distinction that is crucial for interpreting experimental data.

Another way of modeling subdiffusion is via models based on diffusion equations with time-dependent diffusion coefficients [60, 39],

$$(1.8) \quad \frac{\partial p(x, t)}{\partial t} = D(t) \frac{\partial^2 p(x, t)}{\partial x^2}, \quad D(t) \sim t^{\alpha-1}.$$

Although such models reproduce the same MSD scaling as subdiffusive processes, they are primarily phenomenological fitting tools (see [64]). Despite yielding the same probability density as fractional Brownian motion, they lack its correlation structure and are more closely related to mean-field descriptions of CTRW dynamics.

In closing, real systems often exhibit subdiffusion of mixed origin, combining trapping, geometric constraints, and viscoelastic effects. In such cases, different models may predict the same MSD or PDF while differing fundamentally in their aging properties, ergodicity, and trajectory statistics [64].

1.2. Contributions of the paper.

- **Subdiffusion on graphs is a memory-driven process.** Time-fractional diffusion emerges from a random time change that compresses operational time and induces long-tailed waiting times, breaking Markovianity while preserving linearity and mass conservation.
- **Subdiffusion is a superposition of diffusions across multiple time scales.** By using the subordination relation (§2), we approximate the Mittag-Leffler operator by a finite sum of exponential operators (§3). In other words, subdiffusive dynamics admit a representation as a convex and mass-preserving mixture of classical diffusions.
- **Sum-of-exponentials (SOE) approximation bounds.** The error of the discrete SOE approximation decays geometrically (Theorem 3.4). Integral tail bounds and criteria for the selection of the quadrature window are presented in §4.
- **New subdiffusive metric on the graph.** We present a geometrization of the graph based on subdiffusive and diffusive dynamics, analyzing shortest paths between two fixed vertices for those different metrics. Our experiments demonstrate that while diffusive paths explore broader regions of the graph, the subdiffusive regime preserves path history even over extended timescales. (§6)
- **Subdiffusion discovers and remembers topological shortest paths.** We prove that in the small-time limit the subdiffusive shortest paths coincide exactly with the shortest paths in the original metric (Theorems 6.3 and 6.4). This alignment persists over longer timescales, with memory acting as an implicit reinforcement mechanism that suppresses exploration of suboptimal routes and stabilizes optimal trajectories (§6).
- **Subdiffusive geometry selects paths through high-degree regions.** In the small-time limit, we prove that subdiffusive shortest paths favor those topological shortest paths that maximize the average edge degree, reversing classical diffusion’s tendency to avoid hubs and revealing memory-assisted navigation (Theorem 6.3).
- **Memory is heterogeneous and vertex-dependent.** We prove that, although the system is governed by a single fractional order, different vertices (as well as the same vertex at different times) receive larger contributions from remote past, recent past, or present states, depending on the local temporal curvature of the solution (§7).
- **Fractional diffusion induces structural biases absent in classical diffusion.** These include early-time convexity at sources and concavity at neighbors, algebraic (rather than exponential) relaxation, and degree-dependent waiting-time effects fundamentally alter transport, trapping, and path selection on networks (§5 and §8).
- **Fractional dynamics arise as a singular limit of multi-rate diffusion with memory.** Time-fractional equations correspond to scale-free limits of finite superposition of diffusions, equivalently describable

via operator-valued Volterra memory kernels (Proposition 9.2 and Theorem 9.4). This provides a common architecture linking SOE approximations, memory equations, and fractional calculus (§9).

2. PRELIMINARIES

2.1. Notation and assumptions. We work on \mathbb{R}^n with the Euclidean norm $\|\cdot\|_2$ and induced operator norm $\|\cdot\|_2$. We consider $G = (V, E)$ to be a simple undirected graph on n vertices with $A = (A_{ij})$ being its adjacency matrix, and $D = \text{diag}(d_i)$ with $d_i = \sum_j A_{ij}$ the matrix of vertex degree. Let $\mathbb{C}(V)$ be the set of all complex-valued functions on V and let $\ell^2(V)$ be the Hilbert space of square-summable functions on V with inner product:

$$\langle f, g \rangle = \sum_{v \in V} f(v) \overline{g(v)}, \quad f, g \in \ell^2(V).$$

When the graph is finite the Laplacian operator is realized by the so-called graph Laplacian matrix L . $L = D - A$ is real symmetric, positive semidefinite, and $L\mathbf{1} = 0$; if G is connected then $\ker(L) = \text{span}\{\mathbf{1}\}$. The spectrum of L is $0 = \lambda_1 \leq \lambda_2 \leq \dots \leq \lambda_n =: \lambda_{\max}$; let $L = V\Lambda V^\top$ be an orthogonal diagonalization. For a bounded Borel function $f : [0, \infty) \rightarrow \mathbb{R}$ we use the spectral calculus $f(L) := Vf(\Lambda)V^\top$.

If $\{(\lambda_n, \phi_n)\}_{n=1}^N$ are the eigenpairs of L , then the solution of the abstract Cauchy problem of 1.1 is given by

$$\begin{aligned} u(t) &= E_\alpha(-t^\alpha L) u_0 \\ (2.1) \quad &= \sum_{n=1}^N E_\alpha(-\lambda_n t^\alpha) \langle u_0, \phi_n \rangle \phi_n, \end{aligned}$$

where $E_\alpha(M) = E_{\alpha,1}(M)$ is the Mittag-Leffler matrix function of M , which has the following power-series definition:

$$(2.2) \quad E_\alpha(M) = \sum_{k=0}^{\infty} \frac{M^k}{\Gamma(\alpha k + 1)},$$

with $\Gamma(\cdot)$ being the Euler gamma function.

2.2. Subordination identity and the M-Wright density. For $0 < \alpha < 1$,

$$(2.3) \quad E_\alpha(-t^\alpha L) = \int_0^\infty M_\alpha(\theta) e^{-\theta t^\alpha L} d\theta,$$

where $M_\alpha(\theta) \geq 0$ is the M-Wright (Mainardi) density, $\int_0^\infty M_\alpha(\theta) d\theta = 1$, and a convenient series form is [44]

$$(2.4) \quad M_\alpha(\theta) = \sum_{k=0}^{\infty} \frac{(-\theta)^k}{k! \Gamma(1 - \alpha(k + 1))} \quad (\theta \geq 0).$$

The integral in (2.3) is a *Bochner integral* of the operator-valued map $s \mapsto e^{-sL}$ against probability measures. Formally, $(\int e^{-sL} d\mu(s)) u_0$ is the norm-limit of Riemann sums acting on u_0 .

2.3. Complete monotonicity and Bernstein's theorem. The next facts make precise why the fractional propagator is a *positive, mass-preserving* contraction.

Proposition 2.1. *Fix $0 < \alpha < 1$. The scalar function $\lambda \rightarrow E_\alpha(-t^\alpha \lambda)$ is completely monotone on $[0, \infty)$. There is a probability density $M_\alpha(\theta)$ on $(0, \infty)$ such that*

$$E_\alpha(-t^\alpha \lambda) = \int_0^\infty e^{-\theta t^\alpha \lambda} M_\alpha(\theta) d\theta,$$

and in the operator case (Bochner integral):

$$E_\alpha(-t^\alpha L) = \int_0^\infty e^{-\theta t^\alpha L} M_\alpha(\theta) d\theta.$$

Furthermore, $E_\alpha(-t^\alpha L)$ is self-adjoint, positive, and $\|E_\alpha(-t^\alpha L)\|_2 = 1$. Moreover, if $L\mathbf{1} = 0$ then $E_\alpha(-t^\alpha L)\mathbf{1} = \mathbf{1}$.

Proof. The Mittag-Leffler function is completely monotone. By Bernstein's Theorem [61], any completely monotone function can be represented as a mixture of exponentials:

$$E_\alpha(-y) = \int_0^\infty e^{-y\theta} M_\alpha(\theta) d\theta.$$

For the Mittag-Leffler function, the density is given by the Mainardi function $M_\alpha(\theta)$. For a thorough exposition of these results, see [24, 43, 61, 45]. By change of variables $y = t^\alpha \lambda$ we get the desired scalar identity. Functional calculus yields the operator identity:

$$\begin{aligned} E_\alpha(L) &= V E_\alpha(\Lambda) V^\top = V \left(\int_0^\infty e^{-\theta t^\alpha \Lambda} M_\alpha(\theta) d\theta \right) V \\ &= \int_0^\infty \left(V e^{-\theta t^\alpha \Lambda} V \right) M_\alpha(\theta) d\theta = \int_0^\infty e^{-\theta t^\alpha L} M_\alpha(\theta) d\theta. \end{aligned}$$

We have positivity $E_\alpha(-t^\alpha \lambda) \geq 0$ for $0 < \alpha < 1$. From monotonicity we get $E_\alpha(-t^\alpha \lambda) \leq E_\alpha(0) = 1$ for $\lambda \geq 0$. Since L is self-adjoint, the eigenvalues of L are non-negative and $\lambda_1 = 0$, so we have

$$\|E_\alpha(-t^\alpha L)\|_2 = \max_{\lambda \in \sigma(L)} |E_\alpha(-t^\alpha \lambda)| = E_\alpha(0) = 1.$$

The mass property follows from $e^{-\theta t L} \mathbf{1} = \mathbf{1}$ and $\int_0^\infty M_\alpha(\theta) d\theta = 1$. \square

If G is connected, then $\lim_{t \rightarrow \infty} E_\alpha(-t^\alpha L)u_0 = \frac{1}{n}(\mathbf{1}^\top u_0)\mathbf{1}$. For a graph with $c > 1$ components, the limit projects u_0 to the vector that is constant on each component with the corresponding component averages.

2.4. Terminology: subordination and the random clock. Consider the heat semigroup on the graph $\{e^{-sL}\}_{s \geq 0}$. Let $(S_\tau)_{\tau \geq 0}$ be the α -stable subordinator and $E_t = \inf\{\tau > 0 : S_\tau > t\}$ the inverse subordinator. Here, *subordination* means that the time-fractional evolution is obtained by running the baseline (time-linear) heat dynamics with the *random clock* E_t in place of deterministic time,

$$(2.5) \quad E_\alpha(-t^\alpha L) = \int_0^\infty e^{-sL} g_\alpha(s, t) ds = \int_0^\infty M_\alpha(\theta) e^{-\theta t L} d\theta,$$

with $g_\alpha(s, t) = t^{-\alpha} M_\alpha(s/t^\alpha)$; see [50, 2, 45]. We do *not* consider Bochner subordination by a general Bernstein function ϕ (which would lead to space-fractional

$\phi(L)$). Equation (2.5) means that the operator $E_\alpha(-t^\alpha L)$ is the expect value of the standard diffusion operator e^{-sL} , where the $g_\alpha(s, t)$ is the probability that the random clock displays time s when the physical time that has passed is t .

2.5. The time-changed process X_{E_t} . Let $\{X_s\}_{s \geq 0}$ be the continuous-time Markov process on V with generator $-L$:

$$\frac{d}{ds} p(s) = -L p(s), \quad p(s) = (\mathbb{P}[X_s = j \mid X_0 = i])_{i,j} = e^{-sL}.$$

From node i the holding time is an exponential random variable with decay rate $d_i = \sum_j A_{ij}$. The next node is chosen to be j with probability A_{ij}/d_i .

Let $E_t := \inf\{\tau > 0 : S_\tau > t\}$ be the inverse α -stable subordinator ($0 < \alpha < 1$), independent of X . The *time-changed process* is $Y_t := X_{E_t}$, i.e., the baseline diffusion observed at the random operational time E_t .

Averaging over the random clock yields

$$\mathbb{P}[Y_t = j \mid Y_0 = i] = \int_0^\infty \mathbb{P}[X_s = j \mid X_0 = i] g_\alpha(s, t) ds = [E_\alpha(-t^\alpha L)]_{ij}.$$

Hence for any initial u_0 , $u(t) = E_\alpha(-t^\alpha L) u_0$ solves $\partial_t^\alpha u(t) = -Lu(t)$ (Caputo).

Y_t is semi-Markov in physical time t : the holding time T_i at node i has survival $\mathbb{P}(T_i > t) = E_\alpha(-d_i t^\alpha)$, a heavy tail ($\sim t^{-\alpha}$), producing trapping and memory.

Since $L\mathbf{1} = 0$ and the integral representation averages stochastic kernels, Y_t preserves total mass. On a connected graph, $\lim_{t \rightarrow \infty} Y_t$ has the same equilibrium as the baseline walk (componentwise averaging).

3. SUM OF EXPONENTIALS APPROXIMATION

Here we develop a practical, mass-preserving approximation of the Mittag-Leffler function as a sum of exponential functions. We start with the following fundamental definition.

Definition 3.1. The *sum-of-exponentials (SOE)* approximation is

$$(3.1) \quad F_J(t, L) = \sum_{j=1}^J a_j e^{-b_j t^\alpha L},$$

with coefficients a_j, b_j that depend only on α and not on t .

Our aim is to have

$$E_\alpha(-t^\alpha L) \approx \sum_{j=1}^J a_j e^{-b_j t^\alpha L},$$

This approximation is constructed as a quadrature of (2.3) whose window is logarithmically scaled in θ , furthermore we:

- (1) give a log-trapezoidal construction with $a_j > 0$, $\sum_j a_j = 1$ (mass conservation);
- (2) prove geometric convergence in J for a fixed window;
- (3) derive explicit, uniform tail bounds from M_α to select $(\theta_{\min}, \theta_{\max})$;
- (4) tabulate ready-to-use window endpoints $(\theta_{\min}, \theta_{\max})$ (and (y_{\min}, y_{\max})) for typical α, ε ;
- (5) provide practical error metrics (relative/probe, mass error) for a posteriori assessment.

3.1. SOE via log–trapezoidal quadrature. Set $\theta = e^y$, $y \in \mathbb{R}$, and truncate to $[y_{\min}, y_{\max}]$. With a uniform grid $y_j = y_{\min} + (j-1)h$, $h = \frac{y_{\max} - y_{\min}}{J-1}$, define

$$(3.2) \quad b_j = e^{y_j}, \quad \tilde{a}_j = h M_\alpha(b_j) b_j, \quad a_j = \frac{\tilde{a}_j}{\sum_{k=1}^J \tilde{a}_k}.$$

Then

$$(3.3) \quad E_\alpha(-t^\alpha L) \approx \sum_{j=1}^J a_j e^{-b_j t^\alpha L}, \quad a_j > 0, \quad b_j > 0, \quad \sum_{j=1}^J a_j = 1.$$

Convention 1. In all that follows we fix the nodes b_j once (they depend only on α and the chosen log–window) and, for any $t > 0$, we evaluate the SOE as $\sum_{j=1}^J a_j e^{-(t^\alpha b_j) L}$. Thus the coefficients (a_j, b_j) do not depend on t or on L . We then have the following results.

Proposition 3.2. *If $L\mathbf{1} = 0$ and $\sum_j a_j = 1$, then for all $t \geq 0$, $\mathbf{1}^\top (\sum_{j=1}^J a_j e^{-b_j t L}) u_0 = \mathbf{1}^\top u_0$.*

Proof. Since $L\mathbf{1} = 0$, $e^{-b_j t^\alpha L} \mathbf{1} = \mathbf{1}$ for each j . Thus $(\sum_j a_j e^{-b_j t^\alpha L}) \mathbf{1} = (\sum_j a_j) \mathbf{1} = \mathbf{1}$, and left-multiplying by $\mathbf{1}^\top$ gives $\mathbf{1}^\top (\cdot) u_0 = \mathbf{1}^\top u_0$. \square

Lemma 3.3. *For self-adjoint L and bounded Borel f, g , $\|f(L) - g(L)\|_2 = \max_{\lambda \in \sigma(L)} |f(\lambda) - g(\lambda)|$. In particular, the SOE error is*

$$\|E_\alpha(-t^\alpha L) - F_J(t, L)\|_2 = \max_{\lambda \in [0, \lambda_{\max}]} |g(\lambda) - g_J(\lambda)|,$$

with $g(\lambda) = E_\alpha(-t^\alpha \lambda)$ and $g_J(\lambda) = \sum_j a_j e^{-b_j t^\alpha \lambda}$.

Proof. Diagonalize $L = V\Lambda V^\top$. Then $g(L) - g_J(L) = V(g(\Lambda) - g_J(\Lambda))V^\top$ and $\|g(L) - g_J(L)\|_2 = \|g(\Lambda) - g_J(\Lambda)\|_2 = \max_k |g(\lambda_k) - g_J(\lambda_k)|$. \square

Theorem 3.4. *Let $f_\lambda(y) := M_\alpha(e^y) e^y e^{-e^y t^\alpha \lambda}$ with $t > 0$, $\lambda \in [0, \lambda_{\max}]$. For fixed $[y_{\min}, y_{\max}]$ and step $h = (y_{\max} - y_{\min})/(J-1)$,*

$$\sup_{\lambda \in [0, \lambda_{\max}]} \left| \int_{y_{\min}}^{y_{\max}} f_\lambda(y) dy - h \sum_{j=1}^J f_\lambda(y_j) \right| \leq C_1 e^{-C_2/h},$$

with constants $C_1, C_2 > 0$ independent of h and λ . Consequently,

$$\|E_\alpha(-t^\alpha L) - \sum_{j=1}^J a_j e^{-b_j t^\alpha L}\|_2 \leq C_1 e^{-C_2(J-1)/(y_{\max} - y_{\min})}.$$

Proof. (Analytic trapezoidal rule) The map $y \mapsto f_\lambda(y)$ is analytic in a strip $S_a = \{|\operatorname{Im} y| < a\}$ and decays rapidly as $\operatorname{Re} y \rightarrow \pm\infty$ (doubly-exponential decay for $+\infty$, integrable for $-\infty$). For analytic, rapidly decaying functions, the (periodized) trapezoidal rule error on a finite interval is $\leq C e^{-2\pi a/h}$ via Poisson summation; see [69, Thm. 2.1]. Uniform strip bounds in $\lambda \in [0, \lambda_{\max}]$ give uniform C_1, C_2 . Lemma 3.3 transfers the scalar quadrature error to the operator norm bound. \square

3.2. SOE discretization via subordination: quadrature weights, mass preservation, and vertex survivals. We sample uniformly in $y = \log \theta$ on $[y_{\min}, y_{\max}]$ with step

$$h_y = \frac{y_{\max} - y_{\min}}{J-1}, \quad y_j = y_{\min} + (j-1)h_y, \quad b_j = \theta_j = e^{y_j}.$$

The *raw* (log-trapezoid) quadrature weights for the subordination integral are

$$(3.4) \quad w_j^{\text{raw}} = h_y M_\alpha(b_j) b_j \quad (j = 1, \dots, J).$$

They approximate $\int M_\alpha(\theta) (\cdot) d\theta$ on the chosen window, with total mass

$$\text{mass}_{\text{win}} := \sum_{j=1}^J w_j^{\text{raw}} = \int_{\theta_{\min}}^{\theta_{\max}} M_\alpha(\theta) d\theta \leq 1.$$

For the *operator* we enforce mass preservation of the zero mode by normalizing the raw weights,

$$(3.5) \quad a_j = \frac{w_j^{\text{raw}}}{\sum_{k=1}^J w_k^{\text{raw}}}, \quad \sum_{j=1}^J a_j = 1,$$

and keep time only inside the exponentials:

$$(3.6) \quad E_\alpha(-t^\alpha L) \approx \sum_{j=1}^J a_j e^{-(t^\alpha b_j) L}.$$

Here the nodes b_j (internal times θ_j) and the weights depend on α and on the chosen window but are *independent* of t and of L (Convention 1).

Remark 3.5. The normalization (3.5) is essential to preserve mass in the *operator*-level approximation (3.6). For scalar Laplace integrals against M_α one must use the *raw* weights. In particular, the vertex waiting-time survival at node i , with degree $d_i = L_{ii}$,

$$S_i(t) = E_\alpha(-d_i t^\alpha) = \int_0^\infty M_\alpha(\theta) e^{-d_i t^\alpha \theta} d\theta,$$

is approximated by

$$(3.7) \quad S_i(t) \approx \sum_{j=1}^J w_j^{\text{raw}} e^{-(d_i t^\alpha) b_j}.$$

Equivalently, if only the normalized a_j are available,

$$S_i(t) \approx \text{mass}_{\text{win}} \sum_{j=1}^J a_j e^{-(d_i t^\alpha) b_j}, \quad \text{mass}_{\text{win}} = \sum_{j=1}^J w_j^{\text{raw}}.$$

Remark 3.6. Under subordination, θ is the operational (internal) time of the heat semigroup. The SOE nodes $b_j = \theta_j$ are *global internal-time samples*: the same set $\{b_j\}_{j=1}^J$ simultaneously approximates the spectral map $\lambda \mapsto E_\alpha(-(t^\alpha)\lambda)$ (operator level) and all vertex survivals $S_i(t)$ via (3.7). Accuracy is governed by the window $[\theta_{\min}, \theta_{\max}]$: in practice one chooses it using tail bounds so that the peak of $M_\alpha(\theta) e^{-q\theta}$ at $\theta \sim 1/q$ with $q = d_i t^\alpha$ lies well inside the window for all relevant degrees d_i and times t .

4. TAIL BOUNDS FOR THE SUBORDINATION INTEGRAL AND WINDOW SELECTION

Here we start by considering the subordination identity previously defined and its scalar counterpart $F(\lambda) = \int_0^\infty M_\alpha(\theta) e^{-\theta t^\alpha \lambda} d\theta$ for $\lambda \geq 0$. For window endpoints $0 < \theta_{\min} < \theta_{\max} < \infty$ (equivalently, $y_{\min} = \log \theta_{\min}$ and $y_{\max} = \log \theta_{\max}$), we define the truncated operator

$$F_{\text{win}}(L) = \int_{\theta_{\min}}^{\theta_{\max}} M_\alpha(\theta) e^{-\theta t^\alpha L} d\theta,$$

so that the truncation error splits as the *left* and *right* tails:

$$\mathcal{T}_L(\lambda) := \int_0^{\theta_{\min}} M_\alpha(\theta) e^{-\theta t^\alpha \lambda} d\theta, \quad \mathcal{T}_R(\lambda) := \int_{\theta_{\max}}^\infty M_\alpha(\theta) e^{-\theta t^\alpha \lambda} d\theta.$$

By the spectral theorem (Lemma 3.3), the operator truncation error satisfies

$$\|F(L) - F_{\text{win}}(L)\|_2 = \max_{\lambda \in \sigma(L)} (\mathcal{T}_L(\lambda) + \mathcal{T}_R(\lambda)) \leq \sup_{\lambda \in [0, \lambda_{\max}]} \mathcal{T}_L(\lambda) + \sup_{\lambda \in [0, \lambda_{\max}]} \mathcal{T}_R(\lambda).$$

4.1. Left tail (small θ). Near $\theta = 0$, the M-Wright density satisfies $M_\alpha(\theta) = \frac{1}{\Gamma(1-\alpha)} + O(\theta)$ [43, 24]. A simple bound follows.

Proposition 4.1. *For all $t \geq 0$, $\lambda \geq 0$ and $0 < \theta_{\min} \leq 1$,*

$$(4.1) \quad \mathcal{T}_L(\lambda) \leq \frac{1}{\Gamma(1-\alpha)} \begin{cases} \frac{1 - e^{-t^\alpha \lambda \theta_{\min}}}{t^\alpha \lambda}, & \lambda > 0, \\ \theta_{\min}, & \lambda = 0. \end{cases}$$

Consequently, uniformly in $\lambda \in [0, \lambda_{\max}]$,

$$\sup_{\lambda \in [0, \lambda_{\max}]} \mathcal{T}_L(\lambda) \leq \frac{\theta_{\min}}{\Gamma(1-\alpha)}.$$

Proof. Use $M_\alpha(\theta) \leq \frac{1}{\Gamma(1-\alpha)}$ for $\theta \in (0, 1]$ and integrate $\int_0^{\theta_{\min}} e^{-t\lambda\theta} d\theta$ (with the obvious limit as $\lambda \downarrow 0$). \square

We should remark that taking $\theta_{\min} = \varepsilon \Gamma(1-\alpha)$ forces the left-tail contribution below ε for *all* eigenvalues (including the zero mode).

4.2. Right tail (large θ). As $\theta \rightarrow \infty$ the density has a *stretched-exponential* decay [43, Ch. 4], [24, Ch. 2]: there exist $C_\alpha, c_\alpha > 0$ and $q_\alpha := \frac{1}{1-\alpha} > 1$ such that, for all sufficiently large θ ,

$$(4.2) \quad M_\alpha(\theta) \leq C_\alpha \theta^{p_\alpha} \exp(-c_\alpha \theta^{q_\alpha}), \quad p_\alpha := \frac{\alpha-2}{2(1-\alpha)}.$$

This yields two complementary bounds.

Proposition 4.2. *Let (4.2) hold for all $\theta \geq \theta_0(\alpha)$. Then for any $t \geq 0$, $\lambda \geq 0$ and $\theta_{\max} \geq \theta_0(\alpha)$,*

$$(4.3) \quad \mathcal{T}_R(\lambda) \leq \int_{\theta_{\max}}^\infty C_\alpha \theta^{p_\alpha} e^{-c_\alpha \theta^{q_\alpha}} d\theta \leq \frac{C_\alpha}{q_\alpha c_\alpha} \theta_{\max}^{p_\alpha + 1 - q_\alpha} \exp(-c_\alpha \theta_{\max}^{q_\alpha}).$$

In particular, the bound is independent of λ (and thus controls the zero eigenvalue).

Proof. Drop the factor $e^{-t\lambda\theta} \leq 1$ and bound the tail of a monotone stretched-exponential via the standard inequality $\int_x^\infty u^p e^{-cu^q} du \leq \frac{1}{qc} x^{p+1-q} e^{-cx^q}$ for x large. \square

Proposition 4.3. *If the graph is connected and we restrict to $\mathbf{1}^\perp$ (thus $\lambda \geq \lambda_2 > 0$), then for any $\theta_{\max} > 0$,*

$$(4.4) \quad \sup_{\lambda \in [\lambda_2, \lambda_{\max}]} \mathcal{T}_R(\lambda) \leq e^{-t^\alpha \lambda_2 \theta_{\max}} \int_{\theta_{\max}}^\infty M_\alpha(\theta) d\theta \leq e^{-t^\alpha \lambda_2 \theta_{\max}}.$$

Proof. Use $e^{-t\lambda\theta} \leq e^{-t\lambda_2\theta}$ and $\int_{\theta_{\max}}^\infty M_\alpha(\theta) d\theta \leq 1$. \square

We now consider the practical choices based on the previous results:

- *All modes (including $\lambda = 0$):* pick θ_{\max} so that $c_\alpha \theta_{\max}^{q_\alpha} \geq \log(2/\varepsilon)$; then by (4.3), $\sup_\lambda \mathcal{T}_R(\lambda) \lesssim \frac{C_\alpha}{q_\alpha c_\alpha} \theta_{\max}^{p_\alpha + 1 - q_\alpha} e^{-c_\alpha \theta_{\max}^{q_\alpha}} \leq \varepsilon/2$ for large enough θ_{\max} .
- *Mean-zero subspace:* set $\theta_{\max} \geq \frac{1}{t^\alpha \lambda_2} \log(2/\varepsilon)$ to guarantee $\sup_{\lambda \geq \lambda_2} \mathcal{T}_R(\lambda) \leq \varepsilon/2$ by (4.4).

4.3. Putting it together: window rules. Combining Propositions 4.1–4.3 yields explicit choices for $(\theta_{\min}, \theta_{\max})$ ensuring a total tail below a target tolerance ε :

Corollary 4.4. *Given $\varepsilon \in (0, 1)$ and $0 < \alpha < 1$:*

General (all modes). Choose

$$\theta_{\min} = \frac{\varepsilon}{2} \Gamma(1 - \alpha), \quad \theta_{\max} \text{ s.t. } c_\alpha \theta_{\max}^{q_\alpha} \geq \log \frac{2}{\varepsilon}.$$

Then $\sup_{\lambda \in [0, \lambda_{\max}]} (\mathcal{T}_L(\lambda) + \mathcal{T}_R(\lambda)) \leq \varepsilon$.

Mean-zero subspace (connected graph). *If one estimates the operator on $\mathbf{1}^\perp$, take*

$$\theta_{\min} = \frac{\varepsilon}{2} \Gamma(1 - \alpha), \quad \theta_{\max} = \frac{1}{t \lambda_2} \log \frac{2}{\varepsilon}.$$

If one intends to reuse the same nodes for all $t \in [t_{\min}, t_{\max}]$, replace t by t_{\min} in this formula so that (a_j, b_j) are t -independent. Then $\sup_{\lambda \in [\lambda_2, \lambda_{\max}]} (\mathcal{T}_L(\lambda) + \mathcal{T}_R(\lambda)) \leq \varepsilon$.

Remark 4.5. The log–trapezoidal SOE uses $y = \log \theta$ on $[y_{\min}, y_{\max}]$ with $y_{\min} = \log \theta_{\min}$ and $y_{\max} = \log \theta_{\max}$. After fixing the window by Corollary 4.4, increasing J then controls the *discretization* error inside the window with geometric rate (Theorem 3.4).

Remark 4.6. The choice θ_{\max} via Proposition 4.3 with λ_2 replaced by λ_{\max} gives a conservative upper bound on the tail for *high-frequency* modes and motivates rules of the form $\theta_{\max} \sim C/(t\lambda)$. For reuse across multiple times, take $t = t_{\min}$ of the range. Empirically, taking $C \approx 32$ makes $\exp(-\theta_{\max} t \lambda)$ fall near machine precision 10^{-14} and works well when the focus is on modes away from the zero eigenvalue; the rigorous alternative (4.3) controls *all* modes using only properties of M_α .

4.4. Constants in the stretched-exponential bound. Explicit asymptotics for M_α give $q_\alpha = \frac{1}{1-\alpha}$ and an exponent constant $c_\alpha = (1-\alpha) \alpha^{\alpha/(1-\alpha)}$. The prefactor has a power θ^{p_α} with $p_\alpha = \frac{\alpha-2}{2(1-\alpha)}$ and a multiplicative constant depending only on α (see [43, Sec. 4.3] and [24, Sec. 2.3]). Using these in (4.3) yields a fully explicit $\theta_{\max}(\varepsilon, \alpha)$.

5. VERTEX WAITING TIMES AND ERROR METRICS.

In *time-fractional* diffusion, physical time t is linked to the baseline (operational) time s by a *random clock* E_t (the inverse α -stable subordinator, $0 < \alpha < 1$). Its density satisfies the scaling

$$(5.1) \quad g_\alpha(s, t) = t^{-\alpha} M_\alpha\left(\frac{s}{t^\alpha}\right), \quad s > 0, t > 0,$$

and one has the identical subordination forms

$$(5.2) \quad E_\alpha(-t^\alpha L) = \int_0^\infty e^{-sL} g_\alpha(s, t) ds = \int_0^\infty M_\alpha(\theta) e^{-\theta t^\alpha L} d\theta.$$

Let T_i denote the (physical-time) waiting time before the next jump when the process is at node i at time 0. Conditioning on the random clock and averaging yields the *survival function*

$$(5.3) \quad \underbrace{S_i(t)}_{\text{survival}} := \mathbb{P}(T_i > t) = \int_0^\infty e^{-d_i s} g_\alpha(s, t) ds = \int_0^\infty M_\alpha(\theta) e^{-d_i t^\alpha \theta} d\theta = E_\alpha(-d_i t^\alpha), \quad t \geq 0,$$

so each vertex exhibits a *Mittag-Leffler* waiting-time law with heavy tail $S_i(t) \sim (d_i \Gamma(1 - \alpha))^{-1} t^{-\alpha}$.

5.1. Raw vs. normalized quadrature weights. For numerical quadrature on $\theta = e^y$ we use a uniform grid $y_j = y_{\min} + (j - 1)h_y$ with $h_y = (y_{\max} - y_{\min})/(J - 1)$ and set $b_j = \theta_j = e^{y_j}$. The *raw* log-trapezoid weights are

$$w_j^{\text{raw}} = h_y M_\alpha(b_j) b_j, \quad j = 1, \dots, J,$$

which approximate the measure $M_\alpha(\theta) d\theta$ on $[\theta_{\min}, \theta_{\max}]$. Their sum $\text{mass}_{\text{win}} := \sum_j w_j^{\text{raw}} = \int_{\theta_{\min}}^{\theta_{\max}} M_\alpha(\theta) d\theta \leq 1$ is the in-window mass. For the *operator* we normalize to $a_j = w_j^{\text{raw}} / \sum_k w_k^{\text{raw}}$ so that $\sum_j a_j = 1$ and obtain

$$E_\alpha(-t^\alpha L) \approx \sum_{j=1}^J a_j e^{-(t^\alpha b_j)L}.$$

For *scalar* quantities like vertex survivals, probability density functions and hazards, one must use the *raw* weights directly (equivalently, multiply the normalized sums by mass_{win}).

5.2. Mixture interpretation for the random clock. With the raw weights,

$$g_\alpha(s, t) ds \approx \sum_{j=1}^J w_j^{\text{raw}} \delta(s - t b_j) ds,$$

so that, simultaneously for *every* vertex i ,

$$(5.4) \quad S_i(t) \approx \sum_{j=1}^J w_j^{\text{raw}} e^{-d_i t b_j},$$

$$(5.5) \quad f_i(t) := -\frac{d}{dt} S_i(t) \approx d_i \sum_{j=1}^J w_j^{\text{raw}} b_j e^{-d_i t b_j},$$

$$(5.6) \quad h_i(t) := \frac{f_i(t)}{S_i(t)} \approx d_i \frac{\sum_{j=1}^J w_j^{\text{raw}} b_j e^{-d_i t b_j}}{\sum_{j=1}^J w_j^{\text{raw}} e^{-d_i t b_j}} = d_i \frac{\sum_j a_j b_j e^{-d_i t b_j}}{\sum_j a_j e^{-d_i t b_j}}.$$

Then the coefficients w_j^{raw} are the actual “importance” of every exponential term in defining the waiting time at every vertex of the graph.

The SOE internal times $s_j(t) = t b_j$ are *global* operational-time samples drawn from the inverse-stable clock; they are not per-vertex waits. Vertex-dependence enters only through the degree d_i (the baseline attempt rate). Mixing the global internal-time samples with the node-dependent rates d_i yields Mittag-Leffler waiting times at each vertex. In this precise sense, the $\{b_j\}$ are the global internal-time samples whose mixtures simultaneously approximate all vertex waiting-time distributions.

Because (5.4) is a convex combination of decaying exponentials in t , the approximate hazard $h_i(t)$ in (5.6) is a *decreasing* function of t (“aging”), matching the time-fractional renewal interpretation. Also, from $S_i(t) = E_\alpha(-d_i t^\alpha)$ one has $S_i(t) \sim (d_i \Gamma(1-\alpha))^{-1} t^{-\alpha}$ as $t \rightarrow \infty$, so the mean waiting time is infinite for every i when $0 < \alpha < 1$.

5.3. Error metrics. Here we define some error metrics to check the accuracy of the previous approximations. Given a probe vector u_0 and the SOE approximation

$$u^{\text{SOE}}(t) = F_J(t, L) u_0 = \sum_{j=1}^J a_j e^{-b_j t^\alpha L} u_0,$$

we measure the error in the following ways.

5.3.1. Relative error (per probe).

$$(5.7) \quad \text{relerr}(u_0) = \frac{\|u^*(t) - u^{\text{SOE}}(t)\|_2}{\|u^*(t)\|_2}.$$

When multiple probes $\{u_0^{(k)}\}_{k=1}^r$ are used (e.g., random), we report $\max_k \text{relerr}(u_0^{(k)})$.

5.3.2. Mass conservation error.

$$(5.8) \quad \text{masserr}(u_0) = |\mathbf{1}^\top u^*(t) - \mathbf{1}^\top u^{\text{SOE}}(t)|.$$

Ideally $\text{masserr}(u_0) = 0$; with floating-point arithmetic it is typically at the level of machine precision due to $\sum_j a_j = 1$ and $L\mathbf{1} = 0$.

5.3.3. *Scalar error.* The scalar error, intended on the spectrum of the matrix-functions, is

$$(5.9) \quad \max_{\lambda \in [0, \lambda_{\max}]} |E_{\alpha}(-t^{\alpha}\lambda) - F_J(t, \lambda)|.$$

By Theorem 3.4 and uniformly for $\lambda \in [0, \lambda_{\max}]$, the scalar error decays *geometrically* with J once the window captures the effective support of the integrand;

The raw error as a function of J need not be strictly decreasing (typical oscillations of spectrally convergent trapezoidal rules), but its envelope decays until it reaches the desired accuracy [69].

In all cases the SOE inherits the correct long-time limit and conservation properties by construction (Proposition 3.2). Accuracy improves with J and with a window adapted to the relevant scale t, λ .

5.3.4. *Operator error.* If an operator-level diagnostic is desired, one may estimate

$$(5.10) \quad \frac{\|E_{\alpha}(-t^{\alpha}L) - F_J(t, L)\|_2}{\|E_{\alpha}(-t^{\alpha}L)\|_2}$$

via power iteration on the difference operator; in practice, the probe-based relative error (5.7) is sufficient and cheaper.

Note that in exact arithmetic the operator error and the scalar spectral error are the same, since $\|E_{\alpha}(-t^{\alpha}L)\|_2 = 1$ and the 2-norm of the symmetric matrix $E_{\alpha}(-t^{\alpha}L) - F_J(t, L)$ is the magnitude of its largest eigenvalue, which is precisely the scalar error by the spectral theorem applied to the function $g(\lambda) = E_{\alpha}(-t^{\alpha}\lambda) - F_J(t, \lambda)$. However the computation of matrices in floating-point arithmetic may introduce numerical inaccuracies. This can be seen by comparing Fig. 5.1 and Fig. 6.2(B).

5.4. **Computational results.** In this section we consider an Erdős–Rényi (ER) random graph with 250 vertices and 1000 edges. The graph is simple and connected. We then compute the scalar error for three different values of α and a wide range of times $11 \leq t \leq 1001$. The results are illustrated in Fig. 5.1 for $\alpha = 0.8$ (a), $\alpha = 0.5$ (b), and $\alpha = 0.25$ (c). The convergence speed of the scalar error is larger for smaller values of α , that is, fewer addends are needed to obtain a good approximation in the regime of stronger memory effects.

Let us now focus on the nature of the SOE for the three different values of α , with $J = 61$. Using our approach we have the *operator-level* approximations

$$(5.11) \quad E_{0.8}(-t^{0.8}L) \approx 0.242e^{-1.52t^{0.8}L} + 0.220e^{-1.19t^{0.8}L} + 0.148e^{-0.92t^{0.8}L} + \dots,$$

$$(5.12) \quad E_{0.5}(-t^{0.5}L) \approx 0.119e^{-1.48t^{0.5}L} + 0.115e^{-1.15t^{0.5}L} + 0.108e^{-1.90t^{0.5}L} + \dots,$$

and

$$(5.13) \quad E_{0.25}(-t^{0.25}L) \approx 0.096e^{-1.10t^{0.25}L} + 0.095e^{-1.42t^{0.25}L} + 0.091e^{-0.86t^{0.25}L} + \dots.$$

Here each coefficient $a_j > 0$ may be read as the *importance* of the corresponding exponential in the operator mixture; by construction $\sum_j a_j = 1$ so these can also be seen as convex weights. The remaining question is the physical meaning of the rates b_j . For larger values of α , the weight of coefficients is skewed towards one

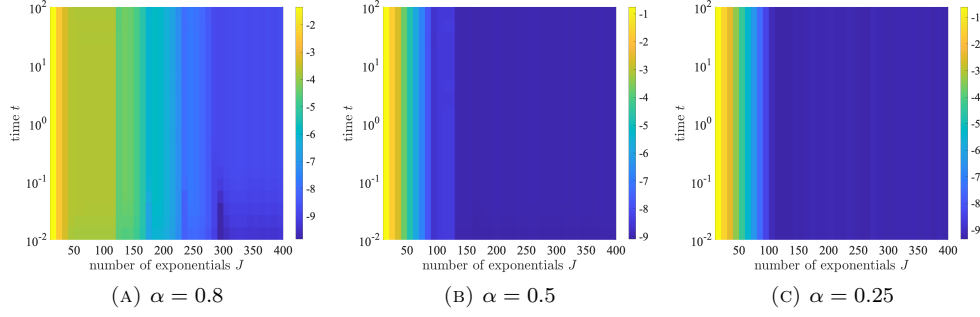


FIGURE 5.1. Base-10 logarithm of the scalar error of the SOE approximation for different times t and number of addends J for an Erdős-Rényi (ER) random graph with 250 vertices and 1000 edges. The plots use $\alpha = 0.8$ (A), $\alpha = 0.5$ (B), and $\alpha = 0.25$ (C).

diffusion. Indeed, in the limit $\alpha \rightarrow 1$, we recover exactly the diffusive behavior, so we expect $a_1 = 1$ and $a_j = 0$ for $j \neq 2$. As α decreases, the contributions of all other diffusions is more prominent. The three leading coefficients in Equation (5.13) indicate that the respective diffusion processes have (almost) the same importance.

To illustrate the importance of the strength of subdiffusion on *vertex waiting times* as previously discussed theoretically in this work let us consider a vertex i of degree one in the ER random graph studied before. Then, for $t = 1$ and $\alpha = 0.8, 0.5, 0.25$ we have the following *survival functions* respectively:

$$\begin{aligned} S_i(0.8, 1) &\approx 0.242e^{-1.52} + 0.220e^{-1.19} + 0.148e^{-0.92} + \dots \approx 0.3869, \\ S_i(0.5, 1) &\approx 0.119e^{-1.48} + 0.115e^{-1.15} + 0.108e^{-1.90} + \dots \approx 0.4276, \\ S_i(0.25, 1) &\approx 0.096e^{-1.10} + 0.095e^{-1.42} + 0.091e^{-0.86} + \dots \approx 0.4639. \end{aligned}$$

As in the approximation of the operator $E_\alpha(-t^\alpha L)$, for large α the weight distribution is skewed toward the waiting time of the most influential distributions. Conversely, as α decreases, the subdiffusive effect is stronger. Particles experience longer residence times at each vertex, before the hop to the next vertex occurs.

What happens for vertices of larger degree? Obviously, the waiting time decreases with the increase of the degree because the diffusive particle has more choices to escape from the vertex. But, why does it also drop with the increase of time? We hypothesize here that the waiting time decreases with the increase of the physical time, because the diffusive particle remembers the paths used previously, such that it has not much to wait to continue a path it already knows.

6. SUBDIFFUSIVE DISTANCE AND PATHS

6.1. Subdiffusive distance. Let us consider the solution of the Caputo time-fractional diffusion equation: $u(t) = E_\alpha(-t^\alpha L) u_0$ in which we consider the initial condition $u_0 = e_v$, where e_v is the vector with one at position v and zero elsewhere. Then, let us consider the capacity of the whole graph to diffuse mass between the vertices v and w at time t . That is, we consider at time t the difference between the mass remaining at the origin, i.e., vertex v , minus the mass diffused to vertex

w:

$$u_{v|u_0=e_v}(t) - u_{w|u_0=e_v}(t) = (E_\alpha(-t^\alpha L))_{vv} - (E_\alpha(-t^\alpha L))_{vw}.$$

Similarly, the capacity of the whole graph to move mass from w to v conditioned to all initial mass being allocated at w is:

$$u_{w|u_0=e_w}(t) - u_{v|u_0=e_w}(t) = (E_\alpha(-t^\alpha L))_{ww} - (E_\alpha(-t^\alpha L))_{vw}.$$

As we only consider undirected graphs here, the total capacity of mass diffusion between both vertices is:

$$(6.1) \quad \mathcal{D}_{\alpha,t}(v, w) = (E_\alpha(-t^\alpha L))_{vv} + (E_\alpha(-t^\alpha L))_{ww} - 2(E_\alpha(-t^\alpha L))_{vw}.$$

Then, we have the following result.

Proposition 6.1. *Let $\mathcal{D}_{\alpha,t}(v, w)$ as defined before. Then $\mathcal{D}_{\alpha,t}(v, w)$ is real and non-negative. There exist an embedding of vertices $V \rightarrow \mathbb{R}^n$, $i \rightarrow x_i$ such that $\mathcal{D}_{\alpha,t}(v, w) = \|x_v - x_w\|_2^2$.*

Proof. Using positivity $E_\alpha(-t^\alpha \lambda) \geq 0$ for $0 < \alpha < 1$ we write

$$\begin{aligned} E_\alpha(-t^\alpha L) &= VE_\alpha(-t^\alpha \Lambda)V^\top \\ &= V(E_\alpha(-t^\alpha \Lambda))^{1/2} (E_\alpha(-t^\alpha \Lambda))^{1/2} V^\top \\ &= (VE_\alpha(-t^\alpha \Lambda))^{1/2} \left((VE_\alpha(-t^\alpha \Lambda))^{1/2} \right)^\top \end{aligned}$$

Denote $X_\alpha(t) = (VE_\alpha(-t^\alpha \Lambda))^{1/2}$ and by $x_{\alpha,t}^\top(v)$ the v -th row of X . Thus,

$$(E_\alpha(-t^\alpha L))_{vw} = x_{\alpha,t}^\top(v) x_{\alpha,t}(w).$$

Then, $v \mapsto x_{\alpha,t}^\top(v)$ is an embedding of vertices in \mathbb{R}^n . Therefore

$$\mathcal{D}_{\alpha,t}(v, w) = \|x_{\alpha,t}(v) - x_{\alpha,t}(w)\|_2^2,$$

so $\mathcal{D}_{\alpha,t}(v, w)$ is a square Euclidean distance between the vertices v and w . \square

Hereafter we call $\mathcal{D}_{\alpha,t}(v, w)$ the (squared) subdiffusive distance between the corresponding vertices in the graph when $\alpha < 1$. Notice that for $\alpha = 1$, the quantity $\mathcal{D}_{1,t}(v, w)$ is the diffusion distance defined by Coiffman et al. [12, 11]. These distances are part of a large family of diffusion-like distances on graphs [15, 18].

6.2. Subdiffusive shortest paths. Instead of considering the subdiffusive distance between any pair of vertices in the graph, which may be adjacent or not, let us instead consider what should be the trajectory of a single subdiffusive particle between two vertices of the graph. In order to compare such trajectories for a standard diffusive particle and a subdiffusive one we define the following general geometrization of the graph (see [46, 7]).

For that purpose we consider every edge $e = (v, w) \in E$ as a compact 1-dimensional manifold with boundary $\partial e = \{v, w\}$. To each edge we assign a time-dependent length

$$W_{\alpha,t}(v, w) = \begin{cases} \sqrt{\mathcal{D}_{\alpha,t}(v, w)}, & (v, w) \in E, \\ 0, & (v, w) \notin E, \end{cases}$$

so that the geometric edge is the interval $\tilde{e}_{\alpha,t}(v, w) = [0, W_{\alpha,t}(v, w)]$. Equipping each edge with this length measure turns the graph into a (time-dependent) metric

length space by extending distances through infima of curve lengths in the associated 1-dimensional complex. In practice we obtain this geometrization by means of the following definition.

Definition 6.2. Let $\sqrt{\mathcal{D}_{\alpha,t}}$ be the matrix of (subdiffusive) distances, intended as the entry-wise square root of $\mathcal{D}_{\alpha,t}$. Define a weighted graph whose adjacency matrix is: $W = A \odot \sqrt{\mathcal{D}_{\alpha,t}}$, which assigns to each edge (i, j) the cost induced by the discrepancy of their diffusion profiles at time t . The resulting weighted graph \tilde{G} is the geometrization of the original graph G .

The resulting shortest paths (computed via Dijkstra's algorithm) identify chains of vertices whose subdiffusion states remain maximally coherent at time t . We dub these paths the *subdiffusive shortest paths*. These paths are not, in general, the paths that require the fewest arcs of A , which we call *topological shortest paths* or *geodesic shortest paths*. They generalize the shortest communicability paths which were introduced in [63] with matrix function $f(A) = \exp(\beta A)$.

Consider the subdiffusive shortest paths on $W(t)$ as time varies. When t is close to zero, the effects of diffusion are minimal. That is, each particle has explored only a small part of the graph. Thus, local properties of the graph are highlighted by the weighted metric. We then have the following two results.

Theorem 6.3 (Shortest-path dominance for the fractional heat kernel as $t \rightarrow 0$). *Let $G = (V, E)$ be a simple undirected graph with combinatorial Laplacian $L = D - A$, and let $0 < \alpha < 1$. Denote by $d(i, j)$ the graph distance between vertices $i \neq j$. Then, for every $i \neq j$,*

$$(E_\alpha(-t^\alpha L))_{ij} = \frac{(-t^\alpha)^{d(i,j)}}{\Gamma(\alpha d(i,j) + 1)} (L^{d(i,j)})_{ij} + O(t^{\alpha(d(i,j)+1)}), \quad t \downarrow 0.$$

In particular,

$$(E_\alpha(-t^\alpha L))_{ij} = O(t^{\alpha d(i,j)}),$$

and the leading-order contribution is determined by topological shortest paths between i and j .

Moreover,

$$(E_\alpha(-t^\alpha L))_{ij} = \frac{t^{\alpha d(i,j)}}{\Gamma(\alpha d(i,j) + 1)} (A^{d(i,j)})_{ij} + O(t^{\alpha(d(i,j)+1)}),$$

where $(A^{d(i,j)})_{ij}$ counts the number of shortest walks of length $d(i, j)$ from i to j .

Proof. The Mittag-Leffler function admits the operator series representation

$$E_\alpha(-t^\alpha L) = \sum_{m=0}^{\infty} \frac{(-t^\alpha)^m}{\Gamma(\alpha m + 1)} L^m,$$

which converges absolutely for all $t \geq 0$ since L is bounded (see, e.g., [52]).

Taking the (i, j) entry yields

$$(E_\alpha(-t^\alpha L))_{ij} = \sum_{m=0}^{\infty} \frac{(-t^\alpha)^m}{\Gamma(\alpha m + 1)} (L^m)_{ij}.$$

As in the classical heat-kernel case, write $L = D - A$. Any term contributing to $(L^m)_{ij}$ corresponds to a product of m factors, each equal to either D or $-A$. Diagonal factors D do not change the vertex index, while each factor A corresponds

to a single edge traversal. Hence, in order for $(L^m)_{ij}$ to be nonzero, the word must contain at least $d(i, j)$ factors of A . Consequently,

$$(L^m)_{ij} = 0 \quad \text{for all } m < d(i, j).$$

For $m = d(i, j)$, the only contributing word is $(-A)^{d(i, j)}$, since any appearance of D would prevent reaching j in exactly $d(i, j)$ steps. Therefore,

$$(L^{d(i, j)})_{ij} = (-1)^{d(i, j)} (A^{d(i, j)})_{ij}.$$

Substituting into the series above, the first nonzero term occurs at $m = d(i, j)$, which proves the stated expansion. \square

Theorem 6.4 (Short-time selection of shortest paths). *Let G be a finite connected graph and let $X(t)$ be the time-fractional continuous-time random walk associated with the Caputo fractional diffusion equation on G (with $0 < \alpha < 1$). Let $N(t)$ be the number of jumps of $X(\cdot)$ up to time t , and let $d(i, j)$ be the graph distance between distinct vertices $i \neq j$. Then, for every $i \neq j$,*

$$\lim_{t \downarrow 0} \mathbb{P}(N(t) = d(i, j) \mid X(t) = j, X(0) = i) = 1.$$

In particular,

$$\lim_{t \downarrow 0} \mathbb{P}(\text{the jump sequence from } i \text{ to } j \text{ up to time } t \text{ has length } d(i, j) \mid X(t) = j, X(0) = i) = 1.$$

That is, conditioned on arrival at j at very short times, the process selects a topological shortest path with probability tending to 1.

Proof. Write $d = d(i, j)$. Let Y_m be the embedded discrete-time jump chain of $X(t)$. The fractional CTRW representation yields

$$\mathbb{P}(X(t) = j \mid X(0) = i) = \sum_{m=0}^{\infty} \mathbb{P}(N(t) = m) \mathbb{P}(Y_m = j \mid Y_0 = i),$$

see [3, 49]. Let P be the one-step transition matrix of Y_m , so that $\mathbb{P}(Y_m = j \mid Y_0 = i) = (P^m)_{ij}$. By definition of graph distance, $(P^m)_{ij} = 0$ for all $m < d$. Hence,

$$\mathbb{P}(X(t) = j \mid X(0) = i) = \sum_{m=d}^{\infty} \mathbb{P}(N(t) = m) (P^m)_{ij}.$$

For the time-fractional walk, the jump-count distribution satisfies the short-time scaling

$$\mathbb{P}(N(t) = m) = \frac{t^{\alpha m}}{\Gamma(\alpha m + 1)} + O(t^{\alpha(m+1)}), \quad t \downarrow 0,$$

see [49]. Therefore the leading contribution comes from $m = d$, and we obtain

$$\mathbb{P}(X(t) = j \mid X(0) = i) = \frac{t^{\alpha d}}{\Gamma(\alpha d + 1)} (P^d)_{ij} + O(t^{\alpha(d+1)}).$$

Similarly,

$$\mathbb{P}(N(t) = d, X(t) = j \mid X(0) = i) = \frac{t^{\alpha d}}{\Gamma(\alpha d + 1)} (P^d)_{ij} + O(t^{\alpha(d+1)}).$$

Dividing the two expansions yields

$$\mathbb{P}(N(t) = d \mid X(t) = j, X(0) = i) = 1 + O(t^\alpha),$$

which proves the claim.

Finally, on the event $\{N(t) = d, X(t) = j, X(0) = i\}$ the jump sequence (Y_0, \dots, Y_d) has length d and connects i to j , hence it is a topological shortest path. \square

Remark 6.5 (Physical interpretation of short-time path selection). The previous results (Theorems 6.3 and 6.4) show that, for both classical and time-fractional diffusion on graphs, the short-time behavior is governed by topological constraints rather than by long-time transport mechanisms. In the fractional case, memory effects and heavy-tailed waiting times manifest themselves through the slower time scaling $t^{\alpha d(i,j)}$ of transition probabilities; however, they do not alter the mechanism by which mass first propagates across the graph. At very short times, the process has insufficient opportunity to perform redundant or backtracking moves, and any realization that reaches a vertex j from i must do so using the minimal number of jumps permitted by the graph distance. Thus, topological shortest paths dominate not because they are energetically or entropically preferred, but because they are the only dynamically admissible routes in the short-time regime. Memory affects *when* such paths become observable, but not *which* paths contribute to the leading-order behavior. This provides a precise mathematical explanation for the observed agreement between diffusion-based distances and graph distances at very small times, even in the presence of anomalous (fractional) temporal dynamics.

Using Theorem 6.3 for two adjacent vertices v, w , we can compute the first-order term of the subdiffusive distance for $t \rightarrow 0$

$$\begin{aligned} \mathcal{D}_{\alpha,t}(v, w) &= E_{\alpha}(-t^{\alpha}L)_{vv} + E_{\alpha}(-t^{\alpha}L)_{ww} - 2E_{\alpha}(-t^{\alpha}L)_{vw} \\ (6.2) \quad &= 2 - \frac{t^{\alpha}}{\Gamma(\alpha+1)}(L_{vv} + L_{ww} - 2L_{vw}) + O(t^{2\alpha}) \\ &= 2 - \frac{t^{\alpha}}{\Gamma(\alpha+1)}(d_v + d_w + 2) + O(t^{2\alpha}). \end{aligned}$$

Note that usually there are multiple topological shortest paths between the same pair of vertices. To understand which of these shortest paths coincides with the subdiffusive shortest path at $t \rightarrow 0$ we find

$$(6.3) \quad W_{\alpha,t}(v, w) = \sqrt{2} - \frac{\sqrt{2}}{4} \frac{t^{\alpha}}{\Gamma(\alpha+1)}(d_v + d_w + 2) + O(t^{2\alpha}).$$

Let P be a path having $m(P)$ edges. In this case the sum of the edge weights in the path is

$$W_{\alpha,t}(P) = \sqrt{2}m(P) \left(1 + \frac{t^{\alpha}}{\Gamma(\alpha+1)}\right) - \frac{\sqrt{2}}{4} \frac{t^{\alpha}}{\Gamma(\alpha+1)} \sum_{k=1}^{m(P)} \delta_{e_k} + O(t^{2\alpha}),$$

where $\delta_{e_k} = d_i + d_j - 2$ is the degree of the edge $e_k = (i, j)$. Consequently, among all the topological shortest paths, the one with the largest sum of edge degrees is chosen by the subdiffusive particle, as it has the smallest subdiffusive length.

6.3. Subdiffusive shortest paths on a geometric graph. We will analyze computationally some of the previous analytical results by considering a Gabriel graph with $n = 600$ vertices and 1156 edges. We use this graph because it is geometric in the sense that its vertices are embedded in \mathbb{R}^d and it can be easily visualized, specially for illustrating paths. Gabriel graphs are defined as follows.

Definition 6.6. Let $P \subset \mathbb{R}^d$ be a finite set of points, referred to as *generators*. The Gabriel graph $G_G = (V_G, E_G)$ associated with P has vertex set $V_G = P$. Two distinct vertices $v, w \in P$ are connected by an edge $\{v, w\} \in E_G$ if and only if the closed ball having the segment $[vw]$ as its diameter contains no other points of P .

In this work, we restrict our attention to the planar case $d = 2$ and use a rectangle with length to width proportion of 2:1 instead of a square to embed the points. We geometrize the Gabriel graph using both the subdiffusive communicability distance $\mathcal{D}_{\alpha,t}(v, w)$ and its sum-of-exponentials (SOE) approximation. Specifically, we use

$$F_J(t, L) = \sum_{j=1}^J a_j e^{-t^\alpha b_j L},$$

and introduce the corresponding approximate squared distance

$$(6.4) \quad \tilde{\mathcal{D}}_{J,\alpha,t}(v, w) = (F_J(t, L))_{vv} + (F_J(t, L))_{ww} - 2(F_J(t, L))_{vw}.$$

Throughout this section, we consider the case $\alpha = 0.85$. Using the square roots of both $\mathcal{D}_{\alpha,t}(v, w)$ and $\tilde{\mathcal{D}}_{J,\alpha,t}(v, w)$, we construct the weighted graph as in Definition 6.2 and compute the subdiffusive shortest paths.

6.3.1. Experimental results. We begin by reporting the topological shortest paths (TSP) between two vertices located near opposite corners of the Gabriel graph (see Fig. 6.1(A)). As is typical—even for planar graphs such as Gabriel graphs—there exist multiple TSPs between a given pair of vertices. These TSPs are colored according to the *average edge degree* along the path, defined as

$$\delta_{e(v,w)} = d_v + d_w - 2,$$

where d_j denotes the degree of vertex j .

We next consider the shortest paths induced by $\tilde{\mathcal{D}}_{J,\alpha,t}(v, w)$ for $J = 1$ (see Fig. 6.1(B)). This case corresponds to a standard diffusive process, since it involves a single exponential term, which is the solution of the classical diffusion equation. We observe that, while at early times the diffusive paths coincide with the TSP as predicted by Theorems 6.3 and 6.4, they progressively deviate as time increases.

As the number of exponentials J in the SOE approximation increases, the corresponding shortest paths converge toward the TSP, as illustrated in panels (C)–(E) of Fig. 6.1. The exact solution based on the Mittag-Leffler function is shown in Fig. 6.1(F), and clearly demonstrates that the subdiffusive shortest paths coincide with the TSPs. Moreover, the limiting paths correspond to those TSPs with the largest average edge degree, in agreement with the analytical results derived in the previous section. Physically, the situation is as follows. At $t \rightarrow 0$ the subdiffusive shortest path coincides with the topological shortest path as proved by Theorems 6.3 and 6.4. However, in the subdiffusive case, as t evolves, the particles remember the previous path used to navigate between two vertices, i.e., the shortest topological path, and repeat it. The result is the repeated use of these paths as shown in Fig. 6.1(F).

The time evolution of the vector probing errors, $\text{relerr}(u_0(t))$ and $\text{masserr}(u_0(t))$, is displayed in Fig. 6.2(A). Fixing J , we can see the mass error decreases with time, while the relative error remains above a certain threshold, which indicates that the two solutions $u^*(t)$ and $u^{\text{SOE}}(t)$ are meaningfully distinct. In Fig. 6.2(B), the time-averages of the vector probing errors and the operator error are plotted as a

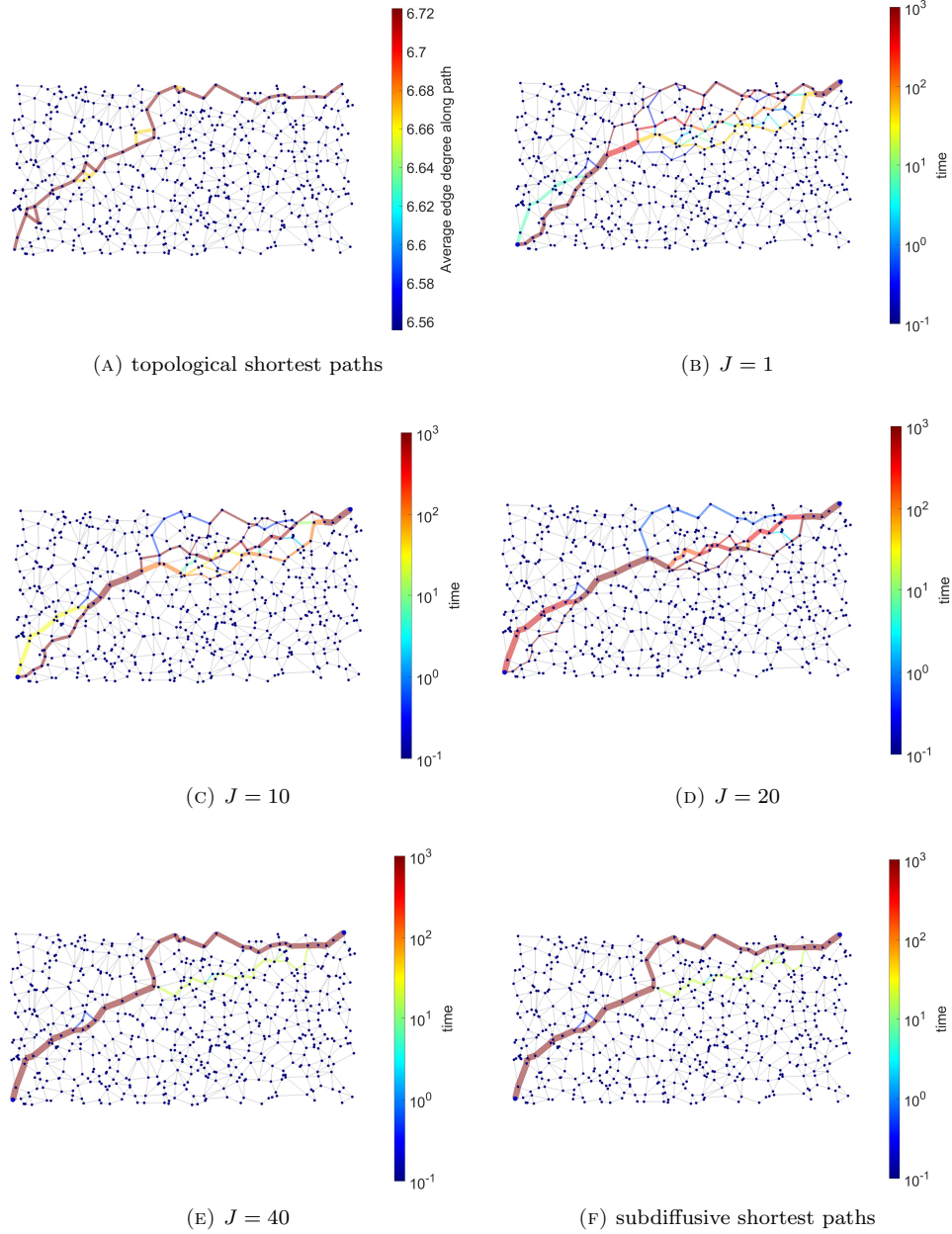


FIGURE 6.1. (A) Illustration of all topological shortest paths between a given pair of vertices in the example Gabriel graph. Coloring is by edge degrees. Shortest paths of SOE approximation for $J = 1, 10, 20, 40$ (B, C, D, E respectively) and $\alpha = 0.85$. (F) Subdiffusive shortest path between the same pair of vertices as before obtained from the Mittag-Leffler function. In (B)-(F) the paths are colored according to the time, which is taken as $0.1 \leq t \leq 1000$ with 300 steps in the interval, at which they are observed and the thickness of the edges is proportional to the number of times they are by the corresponding paths.

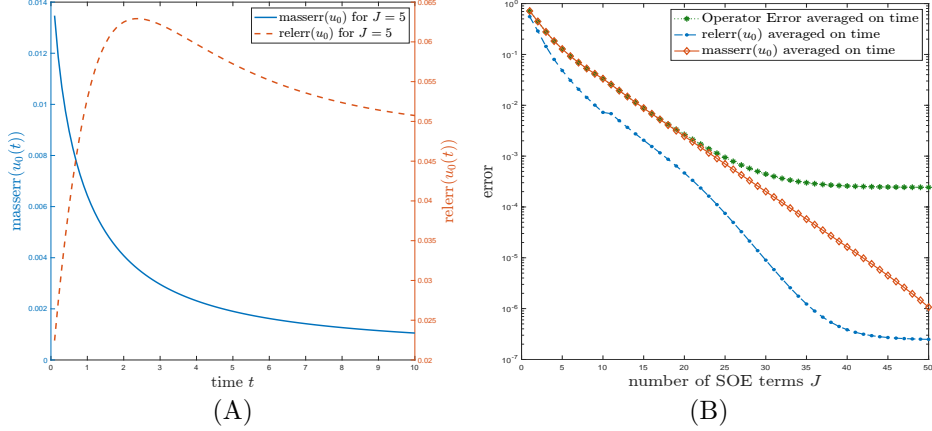


FIGURE 6.2. (A) relative (blue) and mass (orange) errors of the probing vector $u(t)$. Comparison of the solutions dynamics with exact Mittag-Leffler and the SOE approximation with $J = 5$. (B) average on time of the operator (green), relative (blue), and mass (orange) errors as function of J . Average is taken on 300 time instants in the interval $0.1 \leq t \leq 1000$.

function of J . We can see that all the errors decay. The relative and mass errors reach an accuracy of 10^{-9} , while the operator error stagnates 10^{-4} , due to the larger errors in floating-point computations of the operators $F_J(t, L)$.

6.3.2. *Memory reinforcement of past states.* It is clear that increasing J improves the accuracy of the SOE approximation to the Mittag-Leffler function, leading to convergence of the corresponding shortest paths. To interpret this convergence from a physical perspective, recall that the SOE represents a superposition of diffusive processes. Let $b_p = \max\{b_j : 1 \leq j \leq J\}$. Then we can rewrite the SOE operator as

$$(6.5) \quad F_J(t, L) = \sum_{j=1}^J a_j e^{-b_j t^\alpha L} = \sum_{j=1}^J a_j e^{-b_p \frac{b_j}{b_p} t^\alpha L} = \sum_{j=1}^J a_j e^{-b_p t_j^\alpha L},$$

where the effective time instants are given by $t_j = \left(\frac{b_j}{b_p}\right)^{\frac{1}{\alpha}} t$.

In the example graph, the maximum diffusion speed is $b_p = b_2 = 1.53$ (see Table 1). Each term $e^{-b_p t_j^\alpha L}$ therefore represents a diffusion process with speed b_p , evaluated at a slowed time t_j^α . Consequently, subdiffusion can be interpreted not only as a superposition of diffusion processes with different speeds, but also as the sampling of a single diffusion process at multiple past time instants.

This behavior reflects the intrinsic memory property of subdiffusion. Unlike classical diffusion, whose evolution depends solely on the current state, subdiffusive dynamics depend on the entire history of the process. As shown in Fig. 6.1, increasing J incorporates a larger number of past states, allowing the particle to remember its early-time behavior. In this sense, both the Caputo fractional derivative and subdiffusion can be viewed as time-averaged processes over the system's past evolution.

TABLE 1. The largest ten coefficients by magnitude of a_j of the SOE approximation as in the general case of Corollary 4.4 for $\alpha = 0.85$. These coefficients are used for the SOE approximation for the example Gabriel graph are displayed.

j	1	2	3	4	5	6	7	8	9	10
a_j	0.286	0.269	0.167	0.094	0.056	0.035	0.0234	0.016	0.011	0.008
b_j	1.19	1.53	0.93	0.725	0.57	0.44	0.34	0.27	0.21	0.16

The fractional order α controls the strength of this memory effect. As $\alpha \rightarrow 1$, the fractional diffusion equation reduces to the classical diffusion equation, and memory effects vanish. Conversely, as $\alpha \rightarrow 0$, greater weight is assigned to earlier times. This behavior is illustrated in Fig. 6.3, where we plot the dissimilarities of the subdiffusive shortest paths with respect to the topological shortest path for different values of α and J . The dissimilarities are computed with the Levenshtein distance (also known as *edit distance*), which counts the minimum number of edits (insertions, deletions, or substitutions) needed to transform the edge sequence of one path into the other. We observe that smaller values of α require fewer SOE terms to recover the Mittag-Leffler shortest paths. For instance, when $J = 20$, only two distinct paths are observed for $\alpha = 0.25$, whereas multiple paths persist for $\alpha = 0.85$.

The contrast between the diffusive (Fig. 6.1(A)) and subdiffusive (Fig. 6.1(F)) behaviors is striking. When memory is not present, the particles are inclined to explore the graph, as the multiple possible paths show. The incipience of memory allows them to recall the topological shortest path, and gravitate towards it. Memory is strengthened either by lowering the parameter α , or by considering more terms, i.e. by increasing J , as each term is a recall to a previous time instant. Stronger memory means that the Levenshtein distance to the TSP is smaller, as shown in Fig. 6.1.

7. CAPUTO FRACTIONAL DERIVATIVE AND MEMORY

We have seen that memory dictates the behavior of subdiffusion and the underlying fractional-time differential equation. In this section, we analyze the memory contributions present in the Caputo derivative, distinguishing between the influence of the remote past and more recent times. We show an underlying connection between these effects and the convexity of the solution to the subdiffusion equation.

Definition 7.1. Consider the time-fractional Caputo derivative of a function $x(t)$ as defined in §2. For odd k let the interval $[0, t]$ be subdivided into k subintervals $[t_j, t_{j+1}]$ for $j = 0, \dots, k-1$ of equal length $h = t/k$. Let us define the following specific subintervals in $[0, t]$:

- Remote past: $\mathcal{R}(k, \alpha) = \frac{h^{1-\alpha}}{\Gamma(3-\alpha)} \left((k-1)^{2-\alpha} - (k+\alpha-2)k^{1-\alpha} \right) x'(0)$;
- Late past:

$$\mathcal{L}_{\mathcal{R}}(k, \alpha) = \frac{h^{1-\alpha}}{\Gamma(3-\alpha)} \sum_{j=1}^{(k-1)/2} \left((k-j+1)^{2-\alpha} - 2(k-j)^{2-\alpha} + (k-j-1)^{2-\alpha} \right) x'(t_j);$$

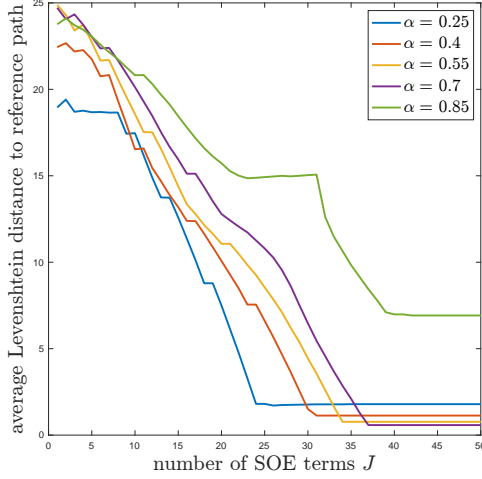


FIGURE 6.3. Comparison of the average Levenshtein distance between the shortest subdiffusive paths and the topological shortest path in the example Gabriel graph, for five values of α . The average is taken on 300 time instants in the interval $0.1 \leq t \leq 1000$.

- Early past:

$$\mathcal{L}_P(k, \alpha) = \frac{h^{1-\alpha}}{\Gamma(3-\alpha)} \sum_{j=(k+1)/2}^{k-1} \left((k-j+1)^{2-\alpha} - 2(k-j)^{2-\alpha} + (k-j-1)^{2-\alpha} \right) x'(t_j);$$

- Present: $\mathcal{P}(t) = \frac{h^{1-\alpha}}{\Gamma(3-\alpha)} x'(t).$

Then, we have the following result proved by Odibat [54].

Theorem 7.2. *The fractional Caputo derivative $D_t^\alpha x(t)$ can be expressed as*

$$(7.1) \quad D_t^\alpha x(t) = \mathcal{R}(k, \alpha) + \mathcal{L}_R(k, \alpha) + \mathcal{L}_P(k, \alpha) + \mathcal{P}(t) - E_C(f, h, \alpha),$$

where $E_C(f, h, \alpha) \leq \mathcal{O}(h^2)$ is the error term.

We have then the following result.

Lemma 7.3. *Let $i \in V$ be a vertex of the graph G . Then, in the limit $\alpha \rightarrow 0$, the contributions for vertex i of the different time subintervals take the values:*

$$\begin{aligned} \mathcal{R}^{(i)}(k, 0) &= \frac{h}{2} x'_i(0), \\ \mathcal{L}_R^{(i)}(k, 0) &= h \sum_{j=1}^{(k-1)/2} x'_i(t_j), \\ \mathcal{L}_P^{(i)}(k, 0) &= h \sum_{j=(k+1)/2}^{k-1} x'_i(t_j), \\ \mathcal{P}^{(i)}(k, 0) &= \frac{h}{2} x'_i(T). \end{aligned}$$

In the limit $\alpha \rightarrow 1$, the only contribution which survives is $\mathcal{P}^{(i)}(k, \alpha \rightarrow 1) = x'_i(T)$ and the rest vanish.

Definition 7.4. For a fixed vertex i , fixed $T > 0$ and odd k , we say that vertex i *recalls its remote past more strongly than its recent past* on $[0, T]$ if

$$\mathcal{L}_{\mathcal{R}}^{(i)}(k, 0) > \mathcal{L}_{\mathcal{P}}^{(i)}(k, 0),$$

and we say it *recalls its recent past more strongly than its remote past* if

$$\mathcal{L}_{\mathcal{R}}^{(i)}(k, 0) < \mathcal{L}_{\mathcal{P}}^{(i)}(k, 0).$$

Theorem 7.5 (Memory Bias). *Let $x(t) = (x_1(t), \dots, x_n(t))^{\top}$ be the solution of the fractional diffusion system with sufficiently smooth temporal evolution at each vertex. Fix a vertex $i \in V$, a time $t > 0$, and an odd integer $k \geq 3$ as above. Then,*

- *If the derivative $x'(t)$ is nonincreasing on $[0, t]$, then*

$$\mathcal{L}_{\mathcal{R}}^{(i)}(k, 0) \geq \mathcal{L}_{\mathcal{P}}^{(i)}(k, 0) \quad \text{and} \quad \mathcal{R}^{(i)}(k, 0) \geq \mathcal{P}^{(i)}(k, 0),$$

and both inequalities are strict if $x'_i(t)$ is strictly decreasing on $[0, t]$. In this case, vertex i recalls its more remote recent past more strongly than its more recent past on $[0, t]$, and it also recalls its remote past more strongly than its present.

- *If the derivative $x'_i(t)$ is nondecreasing on $[0, t]$, then*

$$\mathcal{L}_{\mathcal{R}}^{(i)}(k, 0) \leq \mathcal{L}_{\mathcal{P}}^{(i)}(k, 0) \quad \text{and} \quad \mathcal{R}^{(i)}(k, 0) \leq \mathcal{P}^{(i)}(k, 0),$$

and both inequalities are strict if $x'_i(t)$ is strictly increasing on $[0, t]$. In this case, vertex i recalls its more recent past more strongly than its more remote recent past on $[0, t]$, and it recalls its present more strongly than its remote past.

Proof. The proof is purely temporal and uses only the behavior of $x'_i(t)$ on the interval $[0, t]$; the graph structure enters only through the fact that $x'_i(t)$ arises from the fractional diffusion equation.

Write $k = 2m + 1$, so that $(k - 1)/2 = m$ and $k - 1 = 2m$. For the first part, assume $x'_i(t)$ is nonincreasing on $[0, t]$. Let us compare $\mathcal{L}_{\mathcal{R}}^{(i)}(k, 0)$ and $\mathcal{L}_{\mathcal{P}}^{(i)}(k, 0)$. Define the index reflection $j' = k - j$ for $j = 1, \dots, m$. Then $j' \in \{m + 1, \dots, 2m\}$ and $t_j = jh < j'h = t_{j'}$. By monotonicity, $x'(t_j) \geq x'_i(t_{j'})$. Reindexing the right sum via $j' = k - j$ yields

$$\sum_{j=m+1}^{2m} x'_i(t_j) = \sum_{j=1}^m x'_i(t_{k-j}) = \sum_{j=1}^m x'_i(t_{j'}),$$

so that

$$\sum_{j=1}^m x'_i(t_j) \geq \sum_{j=1}^m x'_i(t_{j'}) = \sum_{j=m+1}^{2m} x'_i(t_j).$$

Multiplying by $h > 0$ yields $\mathcal{L}_{\mathcal{R}}^{(i)}(k, 0) \geq \mathcal{L}_{\mathcal{P}}^{(i)}(k, 0)$, with strict inequality if x'_i is strictly decreasing.

For the comparison between $\mathcal{R}^{(i)}(k, 0)$ and $\mathcal{P}^{(i)}(k, 0)$ we use their explicit expressions

$$\mathcal{R}^{(i)}(k, 0) = \frac{h}{2} x'_i(0), \quad \mathcal{P}^{(i)}(k, 0) = \frac{h}{2} x'_i(T).$$

If $x'_i(t)$ is nonincreasing on $[0, t]$, then $x'_i(0) \geq x'_i(T)$, and multiplying by $h/2 > 0$ gives $\mathcal{R}^{(i)}(k, 0) \geq \mathcal{P}^{(i)}(k, 0)$, with strict inequality if x'_i is strictly decreasing.

For the second part, apply the first part to the function $-x_i(t)$. Denote by $\mathcal{L}_{\mathcal{R}}^{(i)}(k, 0)$ the late past contribution, and similarly for the other time intervals. If $x'_i(t)$ is nondecreasing on $[0, t]$, then $(-x_i)'(t) = -x'_i(t)$ is nonincreasing, hence

$$\mathcal{L}_{\mathcal{R}}^{(i)}(k, 0) \geq \mathcal{L}_{\mathcal{P}}^{(i)}(k, 0) \quad \text{and} \quad \mathcal{R}_{-x_i}^{(i)}(k, 0) \geq \mathcal{P}_{-x_i}^{(i)}(k, 0).$$

By linearity of the sums defining $\mathcal{L}_{\mathcal{R}}$, $\mathcal{L}_{\mathcal{P}}$ and by the explicit formulas for \mathcal{R} and \mathcal{P} ,

$$\begin{aligned} \mathcal{L}_{\mathcal{R}}^{(i)}(k, 0) &= -\mathcal{L}_{\mathcal{R}}^{(i)}(k, 0), & \mathcal{L}_{\mathcal{P}}^{(i)}(k, 0) &= -\mathcal{L}_{\mathcal{P}}^{(i)}(k, 0), \\ \mathcal{R}_{-x_i}^{(i)}(k, 0) &= -\mathcal{R}^{(i)}(k, 0), & \mathcal{P}_{-x_i}^{(i)}(k, 0) &= -\mathcal{P}^{(i)}(k, 0), \end{aligned}$$

and thus

$$-\mathcal{L}_{\mathcal{R}}^{(i)}(k, 0) \geq -\mathcal{L}_{\mathcal{P}}^{(i)}(k, 0), \quad -\mathcal{R}^{(i)}(k, 0) \geq -\mathcal{P}^{(i)}(k, 0),$$

which is equivalent to

$$\mathcal{L}_{\mathcal{R}}^{(i)}(k, 0) \leq \mathcal{L}_{\mathcal{P}}^{(i)}(k, 0), \quad \mathcal{R}^{(i)}(k, 0) \leq \mathcal{P}^{(i)}(k, 0),$$

with strict inequalities if x'_i is strictly increasing. \square

Corollary 7.6. *Under the assumptions of Theorem 7.5, define the total ‘‘past’’ and ‘‘present’’ contributions at vertex i by*

$$\mathcal{T}_{\text{past}}^{(i)}(k, 0) := \mathcal{R}^{(i)}(k, 0) + \mathcal{L}_{\mathcal{R}}^{(i)}(k, 0), \quad \mathcal{T}_{\text{pres}}^{(i)}(k, 0) := \mathcal{L}_{\mathcal{P}}^{(i)}(k, 0) + \mathcal{P}^{(i)}(k, 0).$$

If $x'_i(t)$ is nonincreasing on $[0, t]$, then

$$\mathcal{T}_{\text{past}}^{(i)}(k, 0) \geq \mathcal{T}_{\text{pres}}^{(i)}(k, 0),$$

with strict inequality if x'_i is strictly decreasing. If $x'_i(t)$ is nondecreasing on $[0, t]$, then

$$\mathcal{T}_{\text{past}}^{(i)}(k, 0) \leq \mathcal{T}_{\text{pres}}^{(i)}(k, 0),$$

with strict inequality if x'_i is strictly increasing.

Proof. In the nonincreasing case, Theorem 7.5 yields $\mathcal{R}^{(i)} \geq \mathcal{P}^{(i)}$ and $\mathcal{L}_{\mathcal{R}}^{(i)} \geq \mathcal{L}_{\mathcal{P}}^{(i)}$, so adding the inequalities gives

$$\mathcal{R}^{(i)} + \mathcal{L}_{\mathcal{R}}^{(i)} \geq \mathcal{L}_{\mathcal{P}}^{(i)} + \mathcal{P}^{(i)}.$$

The nondecreasing case is analogous, using the reversed inequalities from Theorem 7.5. \square

Corollary 7.7. *Let $x(t)$ be as in the Caputo fractional diffusion equation, and fix a vertex $i \in V$. Let $[t_1, t_2]$ and $[t_3, t_4]$ be two disjoint time intervals with $0 \leq t_1 < t_2 \leq t_3 < t_4$. Fix an odd integer $k \geq 3$ and define uniform grids on each interval:*

$$h_1 = \frac{t_2 - t_1}{k}, \quad s_j^{(1)} = t_1 + jh_1, \quad j = 0, \dots, k,$$

$$h_2 = \frac{t_4 - t_3}{k}, \quad s_j^{(2)} = t_3 + jh_2, \quad j = 0, \dots, k.$$

Define the corresponding left and right recent contributions:

$$\begin{aligned}\mathcal{L}_{\mathcal{R}}^{(i,1)}(k,0) &:= h_1 \sum_{j=1}^{(k-1)/2} x'_i(s_j^{(1)}), & \mathcal{L}_{\mathcal{P}}^{(i,1)}(k,0) &:= h_1 \sum_{j=(k+1)/2}^{k-1} x'_i(s_j^{(1)}), \\ \mathcal{L}_{\mathcal{R}}^{(i,2)}(k,0) &:= h_2 \sum_{j=1}^{(k-1)/2} x'_i(s_j^{(2)}), & \mathcal{L}_{\mathcal{P}}^{(i,2)}(k,0) &:= h_2 \sum_{j=(k+1)/2}^{k-1} x'_i(s_j^{(2)}).\end{aligned}$$

Assume that

$x'_i(t)$ is strictly decreasing on $[t_1, t_2]$,
 $x'_i(t)$ is strictly increasing on $[t_3, t_4]$.

Then

$$\mathcal{L}_{\mathcal{R}}^{(i,1)}(k,0) > \mathcal{L}_{\mathcal{P}}^{(i,1)}(k,0), \quad \mathcal{L}_{\mathcal{R}}^{(i,2)}(k,0) < \mathcal{L}_{\mathcal{P}}^{(i,2)}(k,0).$$

In particular, on $[t_1, t_2]$ vertex i recalls its more remote recent past more strongly than its more recent past, whereas on $[t_3, t_4]$ the bias is reversed.

Proof. Define $z_1(s) = x_i(t_1 + s)$ on $[0, t_2 - t_1]$ and $z_2(s) = x_i(t_3 + s)$ on $[0, t_4 - t_3]$. Then z'_1 is strictly decreasing and z'_2 is strictly increasing on their respective domains, and the points $s_j^{(1)}, s_j^{(2)}$ define uniform grids. Applying Theorem 7.5 to z_1 and z_2 yields the desired inequalities. \square

Corollary 7.8. Let $x(t)$ be as before, and consider two vertices $i, j \in V$. Fix a time $t > 0$ and an odd integer $k \geq 3$, and define $h = t/k$, $t_\ell = \ell h$ for $\ell = 0, \dots, k$. Define

$$\begin{aligned}\mathcal{L}_{\mathcal{R}}^{(i)}(k,0) &:= h \sum_{\ell=1}^{(k-1)/2} x'_i(t_\ell), & \mathcal{L}_{\mathcal{P}}^{(i)}(k,0) &:= h \sum_{\ell=(k+1)/2}^{k-1} x'_i(t_\ell), \\ \mathcal{L}_{\mathcal{R}}^{(j)}(k,0) &:= h \sum_{\ell=1}^{(k-1)/2} x'_j(t_\ell), & \mathcal{L}_{\mathcal{P}}^{(j)}(k,0) &:= h \sum_{\ell=(k+1)/2}^{k-1} x'_j(t_\ell).\end{aligned}$$

Assume that

$x'_i(t)$ is strictly decreasing on $[0, t]$,
 $x'_j(t)$ is strictly increasing on $[0, t]$.

Then

$$\mathcal{L}_{\mathcal{R}}^{(i)}(k,0) > \mathcal{L}_{\mathcal{P}}^{(i)}(k,0), \quad \mathcal{L}_{\mathcal{R}}^{(j)}(k,0) < \mathcal{L}_{\mathcal{P}}^{(j)}(k,0).$$

Thus, over the same time interval $[0, t]$ and for the same fractional model, vertex i exhibits a remote-past memory bias, whereas vertex j exhibits a recent-past memory bias.

Proof. Apply Theorem 7.5 to the scalar functions $t \mapsto x_i(t)$ and $t \mapsto x_j(t)$ on $[0, t]$. \square

7.1. Physical Interpretation: Memory Regimes on a Graph. The Memory Bias Theorem shows that, within the Caputo-driven fractional diffusion dynamics on a graph for $\alpha \rightarrow 0$, the relative importance of the “remote” versus “recent” parts of the past is not uniform across the network. Instead, it depends sensitively on the *local temporal curvature* of the solution at each vertex.

If the temporal derivative $x'_i(t)$ is decreasing on a given window, the trajectory $x_i(t)$ is bending downward, and older information within that window receives a larger weight than more recent information. In this regime, vertex i is said to exhibit a *remote-past memory bias*. Our results show that, in this case, not only the more remote part of the recent past dominates the more recent part, but the remote past also dominates the present when $\alpha \rightarrow 0$.

Conversely, if $x'_i(t)$ is increasing on a given window, the trajectory is bending upward, and the more recent information receives a larger weight than the more remote information. The vertex then exhibits a *recent-past memory bias*, and in the $\alpha \rightarrow 0$ limit the present dominates the remote past as well.

A striking consequence is that different vertices of the same graph may simultaneously reside in opposite memory regimes, even though they are driven by the same fractional dynamics and are evaluated over the same time interval. Similarly, the *same* vertex may switch memory regimes over time, depending on the evolution of its temporal curvature. This expresses a fundamental “heterogeneity of memory” in fractional diffusion on graphs.

In summary, the fractional order determines *how much* of the past is remembered globally, but the *shape of the temporal evolution* at each vertex dictates *which* part of the past (remote or recent, and past versus present) is preferentially recalled. This creates rich, spatially distributed memory patterns that reflect both the graph geometry and the initial configuration.

8. HOW MEMORY EMERGES FROM FRACTIONAL DIFFUSION ON A GRAPH?

Once we have seen how convexity influences recall of early or late past, we now study how convexity can emerge in a network, depending on the initial mass distribution of the process. The strong influence of memory is also shown through the underlying random clock process.

8.1. Local Convexity and Concavity in Caputo Fractional Diffusion: A Mittag-Leffler and SOE-Based Analysis. We consider the Caputo fractional diffusion equation on a finite graph G with combinatorial Laplacian $L = D - A$:

$$D_t^\alpha x(t) = -Lx(t), \quad x(0) = e_v,$$

where $0 < \alpha < 1$ and e_v is the v th standard basis vector. The mild solution is given by the Mittag-Leffler matrix function

$$x(t) = E_\alpha(-t^\alpha L) e_v.$$

We are interested in the *curvature* of the time evolution at early times, i.e., the sign of $x''_i(t)$ for $t > 0$ sufficiently small. This sign determines whether the temporal trajectory at a vertex is locally convex or concave. We show below that, regardless of the graph, the vertex where the mass is initially placed has an early-time *convex and decreasing* profile, while every neighbor exhibits an early-time *concave and increasing* profile. Both statements hold rigorously for every $0 < \alpha < 1$.

Theorem 8.1 (Local convexity/concavity from Mittag-Leffler and SOE). *Let G be a finite graph with Laplacian $L = D - A$. Consider the Caputo fractional diffusion equation*

$$D_t^\alpha x(t) = -Lx(t), \quad 0 < \alpha < 1, \quad x(0) = e_v.$$

Then:

- At vertex v , the time evolution $x(t)$ is strictly decreasing and strictly convex for all $t \in (0, \varepsilon_v)$, for some $\varepsilon_v > 0$.
- If w is any neighbor of v , i.e. $A_{wv} > 0$, then $x_w(t)$ is strictly increasing and strictly concave for all $t \in (0, \varepsilon_w)$, for some $\varepsilon_w > 0$.

In particular, there exists $\varepsilon > 0$ such that for all $t \in (0, \varepsilon)$ the excited vertex v exhibits a convex decay, while each of its neighbors exhibits a concave growth.

Proof. We use two complementary arguments: (i) the small-time expansion of the Mittag-Leffler matrix function, and (ii) a Sum-of-Exponentials (SOE) representation for E_α .

Step 1: Exact short-time Mittag-Leffler expansion. The matrix Mittag-Leffler function admits the convergent series

$$E_\alpha(-t^\alpha L) = I - \frac{t^\alpha}{\Gamma(\alpha+1)}L + \frac{t^{2\alpha}}{\Gamma(2\alpha+1)}L^2 + O(t^{3\alpha}).$$

Applying this to the initial condition $x(t) = E_\alpha(-t^\alpha L)e_v$ gives

$$x(t) = e_v - \frac{t^\alpha}{\Gamma(\alpha+1)}Le_v + O(t^{2\alpha}).$$

At the excited vertex v we have

$$x_v(t) = 1 - \frac{\deg(v)}{\Gamma(\alpha+1)}t^\alpha + O(t^{2\alpha}),$$

because $(Le_v)_v = \deg(v)$. Differentiating yields

$$x'_v(t) = -\frac{\deg(v)}{\Gamma(\alpha+1)}\alpha t^{\alpha-1} + O(t^{2\alpha-1}) < 0,$$

$$x''_v(t) = -\frac{\deg(v)}{\Gamma(\alpha+1)}\alpha(\alpha-1)t^{\alpha-2} + O(t^{2\alpha-2}) > 0,$$

since $\alpha(\alpha-1) < 0$ for $0 < \alpha < 1$. Note that the exponents $\alpha-1, 2\alpha-2$ are negative. Thus $x_v(t)$ is strictly decreasing and strictly convex on $(0, \varepsilon_v)$.

At a neighbor w of v ,

$$x_w(t) = -\frac{t^\alpha}{\Gamma(\alpha+1)}(Le_v)_w + O(t^{2\alpha}) = \frac{A_{wv}}{\Gamma(\alpha+1)}t^\alpha + O(t^{2\alpha}),$$

because $(Le_v)_w = -A_{wv}$ for $w \neq v$. Thus

$$x'_w(t) = \frac{A_{wv}}{\Gamma(\alpha+1)}\alpha t^{\alpha-1} + O(t^{2\alpha-1}) > 0,$$

$$x''_w(t) = \frac{A_{wv}}{\Gamma(\alpha+1)}\alpha(\alpha-1)t^{\alpha-2} + O(t^{2\alpha-2}) < 0.$$

Hence $x_w(t)$ is strictly increasing and strictly concave on $(0, \varepsilon_w)$.

Step 2: Interpretation via SOE approximation. We have developed a SOE scheme to approximate the Mittag-Leffler function by

$$E_\alpha(-\lambda t^\alpha) \approx \sum_{m=1}^M c_m e^{-d_m t}, \quad c_m > 0, d_m > 0.$$

Applying the same SOE to the matrix L yields

$$x(t) = E_\alpha(-t^\alpha L)e_v \approx \sum_{m=1}^M c_m e^{-d_m t L} e_v.$$

Each term $e^{-d_m t L} e_v$ is the solution of a *classical* diffusion equation with rate d_m and is therefore strictly convex at the source v and strictly concave at neighbors w at early times. Because all coefficients c_m are positive, the SOE sum preserves the convexity at v and concavity at its neighbors. This matches exactly the signs obtained in the rigorous Mittag-Leffler expansion above.

Combining Steps 1 and 2 proves (i) and (ii).

Thus, over the same time interval $t \in (0, \varepsilon_v)$ and for the same fractional model, vertex v exhibits a remote-past memory bias, i.e., it recalls more the past than the present, whereas vertex w exhibits a recent-past memory bias, i.e., it recalls more the present than the past. \square

8.2. Random time change induces subdiffusion and memory. We summarize the mechanism by which the random clock E_t slows down spreading (*subdiffusion*) and introduces *memory* into the dynamics on a graph. Under the subordination identity,

$$u(t) = E_\alpha(-t^\alpha L) u_0 = \mathbb{E}[e^{-E_t L}] u_0,$$

the state at physical time t equals the baseline heat state evaluated at the *random* operational time $s = E_t$. For $0 < \alpha < 1$, the inverse α -stable clock satisfies

$$\mathbb{E}[E_t] = \frac{t^\alpha}{\Gamma(1+\alpha)}, \quad \text{Var}(E_t) = \frac{2t^{2\alpha}}{\Gamma(1+2\alpha)} - \frac{t^{2\alpha}}{\Gamma(1+\alpha)^2},$$

so the *typical* amount of diffusion time available by physical time t scales like t^α (rather than t). Thus any diffusive spread measure that, at baseline, scales with s (e.g., mean-square displacement in Euclidean space, or mixing surrogates on graphs) will scale like t^α under the random clock. This is the essence of *subdiffusion*: slower-than-classical spreading ($t^{\alpha/2}$ instead of $t^{1/2}$ in continuum settings), and on graphs a slower homogenization than the exponential-in- t decay of the standard heat semigroup.

In the time-changed walk $Y_t = X_{E_t}$, the holding time T_i at node i has survival function

$$\mathbb{P}(T_i > t) = E_\alpha(-d_i t^\alpha),$$

with $d_i = \sum_j A_{ij}$. As $t \rightarrow \infty$, the Mittag-Leffler tail obeys $E_\alpha(-d_i t^\alpha) \sim \frac{1}{d_i \Gamma(1-\alpha)} t^{-\alpha}$, a power law (no finite mean inter-jump time when $\alpha < 1$). These *rare but very long* pauses act as traps that stretch physical time relative to operational time, producing subdiffusive spread on the graph.

The Caputo equation

$$\partial_t^\alpha u(t) = -L u(t), \quad \partial_t^\alpha u(t) = \frac{1}{\Gamma(1-\alpha)} \int_0^t (t-\tau)^{-\alpha} u'(\tau) d\tau,$$

is explicitly *history dependent*: the instantaneous rate $u'(t)$ depends on the full past with a power-law kernel $(t-\tau)^{-\alpha}$. In renewal terms, the holding-time hazard for Mittag-Leffler waiting times is *decreasing in age* the longer the process has been waiting, the less likely it is to jump immediately. Hence the future depends on how long the current wait has lasted (“aging”), which breaks the Markov property

in physical time t . Conditioned on $E_t = s$, the baseline path is Markov; *after averaging over* the random clock, the observed dynamics inherit memory.

On the other hand, with $L = V\Lambda V^\top$, each mode decays as

$$E_\alpha(-t^\alpha \lambda_k) \text{ instead of } e^{-t\lambda_k}.$$

For $t \rightarrow \infty$, $E_\alpha(-t^\alpha \lambda_k) \sim \frac{1}{\lambda_k \Gamma(1-\alpha)} t^{-\alpha}$: *algebraic* decay replaces exponential decay. Hence mixing, return probabilities, and any observable built from the heat kernel trace decay more slowly, reflecting both subdiffusion (slower spread) and long memory (long tails). Practical consequences on networks.

- *Slower homogenization*: community imbalances, gradients, or initial heterogeneities persist longer (power-law tail).
- *Trapping in dense/central regions*: large d_i increases the attempt rate, but the heavy-tailed clock still produces long residence episodes; dwell-time distributions are broad across nodes.
- *Non-exponential relaxation*: observables fit Mittag-Leffler or power-law decays rather than exponentials; log–log slopes reveal α .

In summary, the random clock E_t *compresses* operational time from t to t^α on average and introduces *power-law waiting* between moves; together these yield *subdiffusive spreading* and *memory* (aging) in the network dynamics.

9. A GENERALIZED PHYSICO-MATHEMATICAL CONTEXT OF SUBDIFFUSION ON GRAPHS

The fractional-time differential equation that give rise to subdiffusion is widely known. The SOE it is not only the approximation of a function: we show how the superposition of diffusions can emerge in a graph, providing a bridge to graph dynamics, as well as integrating the concepts in the generalized structure of kernel-based differential equations.

9.1. A multiplex diffusion. Let us consider that there are J parallel diffusion processes occurring on the graph G , each of them having a diffusivity constant β_j . Therefore, we can consider a representation of the graph as a multiplex formed by h layers [36, 5], each of them representing the same graph. Every pair of layers l_i and l_j are interconnected by mean of extra edges from a vertex in one layer $v \in l_i$ to itself in another layer $v \in l_j$.

Then, we create the super-Laplacian matrix, which was introduced in [23]:

$$(9.1) \quad \mathfrak{L} = \bigoplus_{j=1}^J \beta_j L + \omega I \otimes (J - I),$$

where \otimes is the Kronecker product, $\omega \in \mathbb{R}^+ \cup \{0\}$ is the strength coupling between the layers, J is an all-ones matrix and I is the identity matrix. Then,

$$(9.2) \quad \mathfrak{L} = \begin{pmatrix} \beta_1 L & C_{12} & \cdots & C_{1J} \\ C_{21} & \beta_2 L & \cdots & C_{2J} \\ \vdots & \vdots & \ddots & \vdots \\ C_{J1} & C_{J2} & \cdots & \beta_J L \end{pmatrix}.$$

Let us write the diffusion equation on the multiplex:

$$(9.3) \quad \partial_t u(t) + \mathfrak{L} u(t) = 0,$$

with initial condition $u(0) = \gamma \otimes \varphi$ where $\gamma = [\gamma_1 \cdots \gamma_J]^T$, $\gamma_j \in \mathbb{R}$ and $\varphi \in \mathbb{R}^{n \times 1}$. The solution of the abstract Cauchy problem is then

$$(9.4) \quad u(t) = e^{-t\mathfrak{L}} u(0).$$

Let us consider a very weak coupling strength between pairs of layers, $\omega \ll 1$, such that we can consider the diffusion at each layer almost independently of the diffusion on other layers:

$$(9.5) \quad u(t) \cong \bigoplus_{j=1}^J \gamma_j e^{-t\beta_j L} \varphi.$$

We then can consider the sum of the concentrations at each vertex of the graph in all layers:

$$(9.6) \quad c(t) = \sum_{j=1}^h u_j(t) = \sum_{j=1}^J \gamma_j e^{-t\beta_j L} \varphi,$$

which is exactly the approximation we have found for the Mittag-Leffler Laplacian function as a SOE. Therefore, the subdiffusive process on the graph can be seen as the total diffusion among the vertices of a graph occurring in parallel at different layers with their own diffusivities and with initial conditions in one layer proportional to the others.

9.2. Factorized high-order temporal diffusion equation. Let us consider h independent diffusive species $v_1(t), \dots, v_J(t) \in \mathbb{R}^n$ evolving according to

$$(9.7) \quad \partial_t v_j(t) + \beta_j L v_j(t) = 0, \quad j = 1, \dots, h,$$

with distinct diffusion rates $\beta_j > 0$. Define the observable field

$$(9.8) \quad u(t) := \sum_{j=1}^J v_j(t).$$

Since L is diagonalizable, it suffices to work in a single Laplacian eigenmode with eigenvalue $\lambda \geq 0$ and corresponding eigenvector $z_\lambda \in \mathbb{R}^n$. Let $x_j(t)$ be the scalar component of $v_j(t)$ relative to the eigenmode λ ; that is, $v_j(t) = \sum_{\lambda \in \text{Sp}(L)} x_j(t) z_\lambda$. Denote $y(t)$ as $y(t) = \sum_{j=1}^J x_j(t)$. The system (9.7) reduces to

$$\partial_t x_j(t) + \beta_j \lambda x_j(t) = 0, \quad j = 1, \dots, h,$$

whose solutions are $x_j(t) = e^{-\beta_j \lambda t} x_j(0)$. Hence

$$y(t) = \sum_{j=1}^J e^{-\beta_j \lambda t} x_j(0).$$

Each exponential $e^{-\beta_j \lambda t}$ is annihilated by the operator $(\partial_t + \beta_j \lambda)$, and therefore

$$\prod_{m=1}^J (\partial_t + \beta_m \lambda) y(t) = 0.$$

Since this holds for every Laplacian eigenvalue λ , we obtain, in operator form, the *multiplicative diffusion equation*

$$(9.9) \quad \prod_{m=1}^J (\partial_t + \beta_m L) u(t) = 0,$$

with suitable initial conditions.

Then, we claim that

$$u(t) = \sum_{j=1}^J \gamma_j e^{-t\beta_j L} \varphi.$$

is an exact solution of the *multiplicative diffusion equation*.

9.2.1. *Verification.* It suffices to check that each term

$$u_j(t) := e^{-t\beta_j L} \varphi$$

lies in the kernel of the operator $\prod_{m=1}^J (\partial_t + \beta_m L)$. First observe that for each fixed m and j ,

$$(\partial_t + \beta_m L) u_j(t) = (-\beta_j L + \beta_m L) e^{-t\beta_j L} \varphi = (\beta_m - \beta_j) L e^{-t\beta_j L} \varphi.$$

Applying the full product, we get

$$\prod_{m=1}^J (\partial_t + \beta_m L) u_j(t) = \left(\prod_{m=1}^J (\beta_m - \beta_j) \right) L^J e^{-t\beta_j L} \varphi.$$

If the β_m are pairwise distinct and $j \in \{1, \dots, h\}$, then one of the factors in the product is $(\beta_j - \beta_j) = 0$. Hence

$$\prod_{m=1}^J (\partial_t + \beta_m L) u_j(t) = 0 \quad \text{for each } j = 1, \dots, h.$$

By linearity,

$$\prod_{m=1}^J (\partial_t + \beta_m L) u(t) = \sum_{j=1}^J \gamma_j \prod_{m=1}^J (\partial_t + \beta_m L) u_j(t) = 0.$$

Thus, the function

$$u(t) = \sum_{j=1}^J \gamma_j e^{-t\beta_j L} \varphi$$

is an exact solution of (9.9).

9.2.2. *Initial conditions.* Equation (9.9) is of order h in time, so one can prescribe $u(0), \partial_t u(0), \dots, \partial_t^{h-1} u(0)$. The representation

$$u(t) = \sum_{j=1}^J e^{-t\beta_j L} \psi_j$$

is the general solution of (9.9), and the vectors ψ_j are uniquely determined from the initial data via a Vandermonde-type linear system (mode by mode in the eigenbasis of L). Choosing

$$\psi_j = \gamma_j \varphi$$

gives precisely

$$u(t) = \sum_{j=1}^J \gamma_j e^{-t\beta_j L} \varphi.$$

Therefore, for any prescribed coefficients β_j , γ_j and profile φ , there exist initial conditions for (9.9) such that the unique solution is exactly

$$u(t) = \sum_{j=1}^J \gamma_j e^{-t\beta_j L} \varphi.$$

9.2.3. Physical interpretation. Equation (9.9) does not describe diffusion of a single species. Rather, it is the *effective evolution equation* satisfied by the total concentration u obtained by summing k independent diffusive species with distinct diffusion rates. The product structure arises from eliminating the hidden fields v_j and encodes the presence of multiple diffusive time scales. Thus, the multiplicative diffusion equation (9.9) represents the minimal closed description of a multi-rate diffusion process when only the aggregate observable is accessible.

9.3. Operator-valued memory and diffusion on graphs.

9.3.1. Operator-valued Volterra kernels. Let X be a finite-dimensional Hilbert space and denote by $\mathcal{L}(X)$ the space of bounded linear operators on X . An *operator-valued Volterra kernel* is a strongly measurable mapping

$$K : \mathbb{R}_+ \rightarrow \mathcal{L}(X)$$

such that

$$\int_0^T \|K(t)\|_{\mathcal{L}(X)} dt < \infty \quad \text{for all } T > 0.$$

Given such a kernel, the associated Volterra convolution operator acts on sufficiently regular functions $u : \mathbb{R}_+ \rightarrow X$ by

$$(\mathcal{K}u)(t) := \int_0^t K(t-s) u(s) ds, \quad t \geq 0.$$

An evolution equation of the form

$$(9.10) \quad u'(t) + \mathcal{K}u(t) = 0$$

is called a *Volterra evolution equation with operator-valued memory*. The Volterra structure enforces causality, while the operator-valued nature of K allows for mode-dependent memory effects.

Remark 9.1. Equation (9.10) describes memory acting directly on the state u . Caputo-type formulations, in which the kernel acts on u' , will arise later as singular limits of this general framework.

9.3.2. *Multiplicative diffusion on graphs.* Let $L \in \mathbb{R}^{n \times n}$ be a symmetric graph Laplacian ($L \succeq 0$ and $\ker L = \text{span}\{\mathbf{1}\}$), and let $\beta_1, \dots, \beta_k > 0$ be pairwise distinct. We consider the *multiplicative diffusion equation*

$$(9.11) \quad \prod_{j=1}^J (\partial_t + \beta_j L) u(t) = 0, \quad t > 0,$$

supplemented with k initial conditions $u(0), u'(0), \dots, u^{(k-1)}(0)$.

Solutions of (9.11) admit the representation

$$(9.12) \quad u(t) = \sum_{j=1}^J e^{-\beta_j t L} \psi_j,$$

where the vectors $\psi_j \in \mathbb{R}^n$ are uniquely determined by the initial conditions. Consequently, the Laplace transform $\widehat{u}(s) = \mathcal{L}\{u\}(s)$ satisfies

$$(9.13) \quad \widehat{u}(s) = \sum_{j=1}^J (sI + \beta_j L)^{-1} \psi_j, \quad u(0) = \sum_{j=1}^J \psi_j.$$

9.3.3. *Equivalence with an operator-valued memory equation.* We now relate (9.11) to a Volterra evolution equation of the form

$$(9.14) \quad u'(t) + \int_0^t K(t-s) L u(s) ds = 0, \quad t > 0,$$

where $K : \mathbb{R}_+ \rightarrow \mathcal{L}(\mathbb{R}^n)$ is an operator-valued Volterra kernel.

Taking the Laplace transform of (9.14) yields

$$(9.15) \quad (sI + \widehat{K}(s)L) \widehat{u}(s) = u(0),$$

for $\Re(s)$ sufficiently large.

Assume for simplicity that $u(0) \in \text{Ran}(L)$, so that L is invertible on the dynamically relevant subspace.¹ Define

$$(9.16) \quad G^{(J)}(s) := \sum_{j=1}^J (sI + \beta_j L)^{-1} P_j,$$

where $P_j : \mathbb{R}^n \rightarrow \mathbb{R}^n$ are linear maps such that $\psi_j = P_j u(0)$. If $G^{(J)}(s)$ is invertible for $\Re(s)$ sufficiently large, define

$$(9.17) \quad \widehat{K}(s) := L^{-1} (G^{(J)}(s)^{-1} - sI).$$

Then (9.13) implies

$$(sI + \widehat{K}(s)L) \widehat{u}(s) = u(0),$$

which coincides with (9.15). Hence, solutions of the multiplicative diffusion equation (9.11) also satisfy the Volterra equation (9.14) with operator-valued kernel K .

¹More generally, L^{-1} may be replaced by the Moore–Penrose inverse L^\dagger .

9.3.4. *Spectral representation.* Let $L = U\Lambda U^\top$ with $\Lambda = \text{diag}(\lambda_\ell)$. On each eigenmode $\lambda > 0$, the kernel is characterized by

$$(9.18) \quad \widehat{K}_\lambda(s) = \frac{1}{\lambda} \left(\frac{1}{\sum_{j=1}^J \frac{p_j(\lambda)}{s+\beta_j \lambda}} - s \right),$$

where $p_j(\lambda)$ are the scalar multipliers induced by P_j . Thus, the memory kernel is generally mode-dependent and cannot be reduced to a single scalar kernel.

9.3.5. *Fractional diffusion as a singular memory limit.* In the next proposition we show that the fractional diffusion equation is equivalent to a Volterra equation, for a suitably chosen subdiffusion kernel K_S .

Proposition 9.2. *Let $L \in \mathbb{R}^{n \times n}$ be a symmetric, positive semidefinite operator (e.g. a graph Laplacian), and let $0 < \alpha < 1$. Consider the Volterra evolution equation*

$$(9.19) \quad u'(t) + \int_0^t K(t-s) L u(s) ds = 0, \quad t > 0,$$

with initial condition $u(0) = u_0$. If the kernel is chosen as

$$(9.20) \quad K_S(t) = \frac{1}{\Gamma(\alpha-1)} t^{\alpha-2}, \quad t > 0,$$

then (9.19) is equivalent to the Caputo fractional diffusion equation

$$(9.21) \quad D_t^\alpha u(t) = -L u(t), \quad t > 0,$$

where D_t^α denotes the Caputo derivative of order α . Moreover, the unique solution is given by

$$(9.22) \quad u(t) = E_\alpha(-t^\alpha L) u_0,$$

where E_α is the Mittag-Leffler function.

Proof. Let $\widehat{u}(s) = \mathcal{L}\{u\}(s)$ denote the Laplace transform of u . Using the identities

$$\mathcal{L}\{u'\}(s) = s\widehat{u}(s) - u_0, \quad \mathcal{L}\left\{\int_0^t K(t-s) L u(s) ds\right\} = \widehat{K}(s) L \widehat{u}(s),$$

the Laplace transform of (9.19) yields

$$(9.23) \quad (sI + \widehat{K}(s)L) \widehat{u}(s) = u_0.$$

For the kernel (9.20), the classical Laplace-transform formula gives

$$\widehat{K}_S(s) = s^{1-\alpha}, \quad \Re(s) > 0.$$

Substituting this expression into (9.23) gives

$$(sI + s^{1-\alpha} L) \widehat{u}(s) = u_0.$$

Multiplying both sides by $s^{\alpha-1}$ yields

$$(9.24) \quad (s^\alpha I + L) \widehat{u}(s) = s^{\alpha-1} u_0$$

On the other hand, the Laplace transform of the Caputo derivative $D_t^\alpha u$ is

$$\mathcal{L}\{D_t^\alpha u\}(s) = s^\alpha \widehat{u}(s) - s^{\alpha-1} u_0.$$

Taking the Laplace transform of (9.21) therefore yields

$$s^\alpha \widehat{u}(s) - s^{\alpha-1} u_0 = -L \widehat{u}(s),$$

which rearranges to (9.24). Thus, equations (9.19) and (9.21) are equivalent.

Finally, the expression of $\hat{u}(s)$ in terms of u_0 can be obtained from (9.24)

$$(9.25) \quad \hat{u}(s) = s^{\alpha-1} (s^\alpha I + L)^{-1} u_0.$$

The inverse Laplace transform of $s^{\alpha-1} (s^\alpha I + L)^{-1}$ is the operator-valued Mittag-Leffler function $E_\alpha(-t^\alpha L)$, which proves (9.22). \square

Remark 9.3. We note that the Laplace-domain representation is written in a *resolvent form*. More generally, finite superpositions of Laplacian semigroups of the form

$$u(t) = \sum_{j=1}^J e^{-\beta_j t L} \psi_j$$

lead (via the construction in §9.18) to operator-valued memory kernels whose Laplace symbols are *rational* in s (mode-by-mode in the spectrum of L). When the number of terms increases and the associated time scales become dense, these rational symbols may converge, in an appropriate sense, to the fractional symbol $s^{\alpha-1}$. In this resolvent sense, time-fractional diffusion can be viewed as a singular, scale-free limit of diffusion with operator-valued Volterra memory.

Note that the kernel $K_S(t)$ is negative, since $0 < \alpha < 1$ and thus $\Gamma(\alpha - 1) < 0$. The stability of the heat Volterra equation has been studied in [40], for a continuous spatial setting, with particular attention to positive and negative kernels. An example of application with a negative kernel in a stochastic setting is given in [25].

Proposition 9.4. *Let $L \in \mathbb{R}^{n \times n}$ be a symmetric graph Laplacian with spectrum $\sigma(L) \subset [0, \lambda_{\max}]$ and let $0 < \alpha < 1$. For s with $\Re(s) > 0$, define the fractional resolvent family*

$$(9.26) \quad \hat{G}_S(s) := s^{\alpha-1} (s^\alpha I + L)^{-1}.$$

Assume that for each $h \in \mathbb{N}$ we are given coefficients $a_j, b_j > 0$ ($j = 1, \dots, h$) and define the rational operator-valued symbol

$$(9.27) \quad \hat{G}^{(J)}(s) := \sum_{j=1}^J a_j (sI + b_j L)^{-1}.$$

Suppose there exists a domain $\Omega \subset \{s \in \mathbb{C} : \Re(s) > 0\}$ and constants $M, \delta > 0$ such that for all $s \in \Omega$:

$$(9.28) \quad \|\hat{G}_S(s)\| \leq M,$$

$$(9.29) \quad \|\hat{G}_S(s)^{-1}\|_{\text{Ran}(L) \rightarrow \text{Ran}(L)} \leq M,$$

$$(9.30) \quad \|\hat{G}^{(J)}(s) - \hat{G}_S(s)\| \leq \delta, \quad \text{with } \delta M < 1.$$

(Here $\hat{G}_S(s)^{-1}$ denotes the inverse on $\text{Ran}(L)$, and the norm is the operator norm on \mathbb{R}^n .)

Then for every $s \in \Omega$:

$\hat{G}^{(J)}(s)$ is invertible on $\text{Ran}(L)$ and

$$(9.31) \quad \|\hat{G}^{(J)}(s)^{-1} - \hat{G}_S(s)^{-1}\|_{\text{Ran}(L) \rightarrow \text{Ran}(L)} \leq \frac{M^2}{1 - \delta M} \|\hat{G}^{(J)}(s) - \hat{G}_S(s)\|.$$

Define the SOE-induced operator-valued memory symbol by

$$(9.32) \quad \hat{K}^{(J)}(s) := (\hat{G}^{(J)}(s)^{-1} - sI)L^\dagger, \quad s \in \Omega,$$

where L^\dagger is the Moore-Penrose inverse. Define analogously

$$(9.33) \quad \hat{K}_S(s) := (\hat{G}_S(s)^{-1} - sI)L^\dagger = s^{1-\alpha}I \quad \text{on } \text{Ran}(L).$$

Then

$$(9.34) \quad (sI + \hat{K}^{(J)}(s)L)^{-1} = \hat{G}^{(J)}(s), \quad (sI + \hat{K}_S(s)L)^{-1} = \hat{G}_S(s),$$

and moreover the resolvents converge in operator norm:

$$(9.35) \quad \|(sI + \hat{K}^{(J)}(s)L)^{-1} - (sI + s^{\alpha-1}L)^{-1}\| = \|\hat{G}^{(J)}(s) - \hat{G}_S(s)\| \xrightarrow[J \rightarrow \infty]{} 0, \quad s \in \Omega.$$

Proof. Fix $s \in \Omega$.

Step 1: stability of invertibility on $\text{Ran}(L)$. Let $A := \hat{G}_S(s)$ and $B := \hat{G}^{(J)}(s)$, viewed as operators on $\text{Ran}(L)$. By assumption A is invertible there and $\|A^{-1}\| \leq M$. Moreover,

$$\|A^{-1}(B - A)\| \leq \|A^{-1}\| \|B - A\| \leq M\delta < 1.$$

Hence B is invertible on $\text{Ran}(L)$ and the standard resolvent identity gives

$$B^{-1} - A^{-1} = B^{-1}(A - B)A^{-1}.$$

Using $\|B^{-1}\| \leq \|A^{-1}\|/(1 - \|A^{-1}(B - A)\|) \leq M/(1 - \delta M)$, we obtain

$$\|B^{-1} - A^{-1}\| \leq \frac{M}{1 - \delta M} \|A - B\| M = \frac{M^2}{1 - \delta M} \|B - A\|,$$

which proves (9.31).

Step 2: definition of the memory symbols and resolvent identities. By definition (9.32),

$$\hat{G}^{(J)}(s)^{-1} = sI + \hat{K}^{(J)}(s)L \quad \text{on } \text{Ran}(L),$$

because $L^\dagger L$ is the identity on $\text{Ran}(L)$. Taking inverses on $\text{Ran}(L)$ yields

$$(sI + \hat{K}^{(J)}(s)L)^{-1} = \hat{G}^{(J)}(s) \quad \text{on } \text{Ran}(L),$$

and the same argument gives $(sI + \hat{K}_S(s)L)^{-1} = \hat{G}_S(s)$. This proves (9.34).

Step 3: identifying $\hat{K}_S(s)$ and resolvent convergence. From (9.26) we have

$$\hat{G}_S(s)^{-1} = s^{1-\alpha}(s^\alpha I + L) = sI + s^{1-\alpha}L,$$

hence $\hat{K}_S(s) = s^{\alpha-1}I$ as in (9.33) on $\text{Ran}(L)$. Therefore,

$$(sI + \hat{K}_S(s)L)^{-1} = (sI + s^{1-\alpha}L)^{-1} = \hat{G}_S(s).$$

Finally, (9.35) follows immediately from (9.34) and the assumed closeness (9.30), and in particular tends to 0 if $\|\hat{G}^{(J)}(s) - \hat{G}_S(s)\| \rightarrow 0$ as $J \rightarrow \infty$. \square

An analysis of the subdiffusion equation with memory with relation to rational kernels in the Laplace-domain can be found in [57].

Remark 9.5. Theorem 9.4 provides a precise way to say that an SOE approximation does not merely approximate a solution curve, but induces an *approximate evolution law* in the same analytic class as the limiting fractional dynamics, namely through the Laplace-domain resolvent. It makes explicit the structural pathway

$$\boxed{\text{SOE} \quad \iff \quad \text{operator-valued} \quad \implies \quad \text{fractional limit}}$$

where the double arrow refers to the exact algebraic construction $\widehat{G}^{(J)} \leftrightarrow \widehat{K}^{(J)}$ via (9.32) and (9.34), while the single arrow denotes the limiting process $J \rightarrow \infty$ in the resolvent sense (9.35). This is the natural notion of convergence for nonlocal-in-time equations, since the resolvent family uniquely characterizes the corresponding linear evolution.

Remark 9.6. The conclusions of Theorem 9.4 are restricted to *Laplace-domain* (resolvent) statements on a domain $\Omega \subset \{\Re(s) > 0\}$. In particular, the proposition does *not* assert any of the following:

Time-domain kernel convergence. It does not claim that the inverse Laplace transforms satisfy $K^{(J)}(t) \rightarrow K_S(t)$ pointwise, in $L^1_{\text{loc}}(\mathbb{R}_+)$, or in any distributional sense.

Strong convergence of semigroup families in physical time. If a physical-time representation involves nonlinear reparametrizations (e.g. $\tau = t^\alpha$), the proposition does not claim that uniform approximation of $G^{(J)}(\tau)$ implies convergence of Laplace transforms in the physical time variable.

Equivalence to a Caputo equation for each finite J . For finite J , the induced kernel is regular (typically a finite exponential mixture in time), and the proposition does not claim that the corresponding memory equation is a Caputo fractional differential equation.

Global-in- s convergence. No statement is made about convergence uniformly for all $\Re(s) > 0$, nor about behavior near $s = 0$ or $|s| \rightarrow \infty$ unless such regions are included in Ω and the hypotheses are verified there.

CONCLUSIONS

In this work we have investigated subdiffusion on graphs from a structural, dynamical, and mechanistic perspective, emphasizing the role of memory rather than modifying spatial connectivity or transition rules. By grounding time-fractional diffusion in a random time-change framework, we have shown that subdiffusion on networks is not merely a slower version of classical diffusion, but a fundamentally non-Markovian process in which past states actively shape future evolution. Importantly, this loss of Markovianity occurs without sacrificing linearity or mass conservation, making time-fractional models both analytically tractable and physically meaningful for networked systems.

A central outcome of our analysis is the demonstration that Mittag-Leffler graph dynamics admit a convex, mass-preserving decomposition into a finite or infinite superposition of classical heat semigroups evaluated at rescaled times. This representation provides a transparent interpretation of subdiffusion as a multi-time-scale diffusion process and forms the basis for efficient numerical approximations via sum-of-exponentials schemes. Beyond computational convenience, this viewpoint reveals how memory operates at the operator level and clarifies the relationship between

fractional dynamics, diffusion with memory kernels, and multi-rate transport processes.

At the vertex level, we have shown that memory in fractional diffusion is inherently heterogeneous. Despite being governed by a single fractional order, different nodes—and even the same node at different times—exhibit distinct memory biases, favoring remote past, recent past, or present contributions depending on the local temporal curvature of the evolving state. This heterogeneity is absent in classical diffusion and highlights how fractional dynamics encode rich, spatially distributed memory patterns that reflect both network structure and initial conditions.

These memory effects have concrete consequences for transport and geometry on graphs. Fractional diffusion induces qualitative biases such as early-time convex decay at sources, concave growth at neighbors, algebraic relaxation of modes, and degree-dependent waiting times. Together, these features reshape how mass propagates through the network, altering trapping behavior and path selection in ways that cannot be captured by Markovian models.

Perhaps most strikingly, we have shown that subdiffusive dynamics enable a particle to discover shortest topological paths between vertices using only local information. Memory acts as an implicit reinforcement mechanism that suppresses exploration of suboptimal routes and stabilizes optimal trajectories, leading shortest subdiffusive paths to coincide with shortest topological paths. Moreover, among these, subdiffusion preferentially selects paths traversing high-degree regions, reversing the hub-avoidance tendency of classical diffusion and revealing a form of memory-assisted navigation on networks.

Finally, by connecting fractional diffusion to finite superpositions of classical diffusions and to operator-valued Volterra memory equations, we have placed time-fractional graph dynamics within a broader hierarchy of diffusion models with memory. In this view, fractional equations arise as singular, scale-free limits of multi-rate processes, providing a unifying framework that links analytical theory, numerical approximation, and physical interpretation. Taken together, our results clarify what subdiffusion means on a graph, how memory reshapes network transport, and why fractional dynamics constitute a natural and structurally rich extension of classical diffusion on networks.

10. APPENDIX

10.0.1. *Numerical window tables and usage.* We summarize practical window choices for the log–trapezoidal SOE, based on the tail bounds previously found. For the *right tail*, the stretched–exponential decay of M_α implies that

$$\theta_{\max} \geq \left(\frac{\log(2/\varepsilon)}{c_\alpha} \right)^{1/q_\alpha}, \quad c_\alpha = (1-\alpha) \alpha^{\alpha/(1-\alpha)}, \quad q_\alpha = \frac{1}{1-\alpha},$$

is sufficient to make $\sup_{\lambda \in [0, \lambda_{\max}]} \int_{\theta_{\max}}^{\infty} M_\alpha(\theta) e^{-\theta t \lambda} d\theta \lesssim \varepsilon/2$ uniformly in λ (i.e., including the zero mode); see (4.3). For the *left tail*, taking $\theta_{\min} = \frac{\varepsilon}{2} \Gamma(1-\alpha)$ ensures $\sup_{\lambda \in [0, \lambda_{\max}]} \int_0^{\theta_{\min}} M_\alpha(\theta) e^{-\theta t \lambda} d\theta \leq \varepsilon/2$ (Prop. 4.1).

Tables 2–3 list these cutoffs for typical α and ε values, together with $y_{\max} = \log \theta_{\max}$ and $y_{\min} = \log \theta_{\min}$, which are the actual endpoints used by the SOE in the variable $y = \log \theta$.

α	$\varepsilon = 10^{-6}$	$\varepsilon = 10^{-8}$	$\varepsilon = 10^{-10}$	$\varepsilon = 10^{-12}$
0.20	14.016 [2.640]	17.474 [2.861]	20.768 [3.033]	23.936 [3.175]
0.30	11.979 [2.483]	14.529 [2.676]	16.899 [2.827]	19.134 [2.951]
0.50	7.618 [2.031]	8.744 [2.168]	9.740 [2.276]	10.644 [2.365]
0.70	4.109 [1.413]	4.464 [1.496]	4.762 [1.561]	5.023 [1.614]
0.80	2.816 [1.035]	2.976 [1.090]	3.107 [1.134]	3.219 [1.169]

TABLE 2. Conservative right-tail cutoff θ_{\max} ensuring $\sup_{\lambda \in [0, \lambda_{\max}]} \int_{\theta_{\max}}^{\infty} M_{\alpha}(\theta) e^{-\theta t \lambda} d\theta \lesssim \varepsilon/2$. Brackets show $y_{\max} = \log \theta_{\max}$ for direct use in the log-trapezoidal SOE. Values are *independent* of t and of the spectrum; they come from the uniform bound (4.3) using the stretched-exponential tail of M_{α} with constants c_{α}, q_{α} [43, 24].

α	$\varepsilon = 10^{-6}$	$\varepsilon = 10^{-8}$	$\varepsilon = 10^{-10}$	$\varepsilon = 10^{-12}$
0.20	5.82×10^{-7} [-14.357]	5.82×10^{-9} [-18.962]	5.82×10^{-11} [-23.567]	5.82×10^{-13} [-28.172]
0.30	6.49×10^{-7} [-14.248]	6.49×10^{-9} [-18.853]	6.49×10^{-11} [-23.458]	6.49×10^{-13} [-28.063]
0.50	8.86×10^{-7} [-13.936]	8.86×10^{-9} [-18.541]	8.86×10^{-11} [-23.147]	8.86×10^{-13} [-27.752]
0.70	1.50×10^{-6} [-13.413]	1.50×10^{-8} [-18.018]	1.50×10^{-10} [-22.623]	1.50×10^{-12} [-27.228]
0.80	2.30×10^{-6} [-12.985]	2.30×10^{-8} [-17.590]	2.30×10^{-10} [-22.195]	2.30×10^{-12} [-26.800]

TABLE 3. Left-tail cutoff $\theta_{\min} = \frac{\varepsilon}{2} \Gamma(1 - \alpha)$ guaranteeing $\sup_{\lambda \in [0, \lambda_{\max}]} \int_0^{\theta_{\min}} M_{\alpha}(\theta) e^{-\theta t \lambda} d\theta \leq \varepsilon/2$. Brackets show $y_{\min} = \log \theta_{\min}$. (Rounded to three significant digits.)

Let us now explain how to use these Tables.

- (1) Fix a target tolerance ε for the *tails* (e.g., $\varepsilon = 10^{-12}$ in double precision).
- (2) Read off $(\theta_{\min}, y_{\min})$ from Table 3 and $(\theta_{\max}, y_{\max})$ from Table 2 for your α and ε .
- (3) Set the SOE window in the log variable as $[y_{\min}, y_{\max}]$; then increase J until the *in-window discretization* error decays to your overall tolerance (Theorem 3.4 shows geometric decay with J).

Variants and remarks.

- (*Mean-zero subspace.*) If you only act on $\mathbf{1}^{\perp}$ and know the spectral gap $\lambda_2 > 0$, you may choose $\theta_{\max} = \frac{1}{t \lambda_2} \log(2/\varepsilon)$ (for reuse over $t \in [t_{\min}, t_{\max}]$, use t_{\min} here to keep the nodes t -independent) (Prop. 4.3), which can be *much smaller* than the uniform value in Table 2.
- (*Heuristic rule of thumb.*) For high-frequency modes it is common to take $\theta_{\max} \approx \frac{32}{t \lambda}$ so that $e^{-\theta_{\max} t \lambda} \approx 10^{-14}$ (machine precision). The uniform bound above is conservative and includes the zero mode.
- (*Scaling with α .*) As $\alpha \uparrow 1$ the tail constant c_{α} grows and the required θ_{\max} shrinks; as $\alpha \downarrow 0$ the reverse happens, hence the larger values in the top row of Table 2.

Acknowledgments: E.E. thanks financial support from Agencia Estatal de Investigación (AEI, MCI, Spain) MCIN/AEI/ 10.13039/501100011033 under grant PID2023-149473NB-I00 and by Agencia Estatal de Investigación (AEI, MCI, Spain) MCIN/AEI/ 10.13039/501100011033 and Fondo Europeo de Desarrollo Regional (FEDER, UE) under the María de Maeztu Program for units of Excellence in R&D, grant CEX2021-001164-M) are also acknowledged.

REFERENCES

- [1] Luciano Abadias, Gissell Estrada-Rodriguez, and Ernesto Estrada. Fractional-order susceptible-infected model: definition and applications to the study of covid-19 main protease. *Fractional Calculus and Applied Analysis*, 23(3):635–655, 2020.
- [2] David Applebaum. *Lévy Processes and Stochastic Calculus*, volume 116 of *Cambridge Studies in Advanced Mathematics*. Cambridge University Press, Cambridge, 2 edition, 2009.
- [3] Boris Baeumer and Mark M. Meerschaert. Stochastic solutions for fractional cauchy problems. *Fractional Calculus and Applied Analysis*, 4(4):481–500, 2001.
- [4] Sujit Basak, Sombuddha Sengupta, and Krishnananda Chattopadhyay. Understanding biochemical processes in the presence of sub-diffusive behavior of biomolecules in solution and living cells. *Biophysical Reviews*, 11(6):851–872, 2019.
- [5] Stefano Boccaletti, Ginestra Bianconi, Regino Criado, Charo I Del Genio, Jesús Gómez-Gardenes, Miguel Romance, Irene Sendina-Nadal, Zhen Wang, and Massimiliano Zanin. The structure and dynamics of multilayer networks. *Physics reports*, 544(1):1–122, 2014.
- [6] Jean-Philippe Bouchaud and Antoine Georges. Anomalous diffusion in disordered media: statistical mechanisms, models and physical applications. *Physics reports*, 195(4-5):127–293, 1990.
- [7] Martin R Bridson and André Haefliger. *Metric spaces of non-positive curvature*, volume 319. Springer Science & Business Media, 2013.
- [8] Yongcan Cao, Yan Li, Wei Ren, and YangQuan Chen. Distributed coordination of networked fractional-order systems. *IEEE Transactions on Systems, Man, and Cybernetics, Part B (Cybernetics)*, 40(2):362–370, 2009.
- [9] Michele Caputo. Linear models of dissipation whose q is almost frequency independent. *Annals of Geophysics*, 19(4):383–393, 1966.
- [10] Tanisha Chauhan, Kaushik Kalyanaraman, and Sarthok Sircar. Quantifying macrostructures in viscoelastic sub-diffusive flows. *Journal of Mathematical Physics*, 65(7), 2024.
- [11] Ronald R Coifman and Stéphane Lafon. Diffusion maps. *Applied and computational harmonic analysis*, 21(1):5–30, 2006.
- [12] Ronald R Coifman, Stephane Lafon, Ann B Lee, Mauro Maggioni, Boaz Nadler, Frederick Warner, and Steven W Zucker. Geometric diffusions as a tool for harmonic analysis and structure definition of data: Diffusion maps. *Proceedings of the national academy of sciences*, 102(21):7426–7431, 2005.
- [13] Jay Samuel L Combinido and May T Lim. Crowding effects in vehicular traffic. *Plos one*, 7(11):e48151, 2012.
- [14] Matteo D’Alessandro and Piet Van Mieghem. Fractional derivative in continuous-time markov processes and applications to epidemics in networks. *Physical Review Research*, 7(1):013017, 2025.
- [15] Ernesto Estrada. The communicability distance in graphs. *Linear Algebra and its Applications*, 436(11):4317–4328, 2012.
- [16] Ernesto Estrada. *The structure of complex networks: theory and applications*. Oxford University Press, 2012.
- [17] Ernesto Estrada. Fractional diffusion on the human proteome as an alternative to the multi-organ damage of sars-cov-2. *Chaos: An Interdisciplinary Journal of Nonlinear Science*, 30(8), 2020.
- [18] Ernesto Estrada, MG Sanchez-Lirola, and José Antonio De La Peña. Hyperspherical embedding of graphs and networks in communicability spaces. *Discrete Applied Mathematics*, 176:53–77, 2014.
- [19] Luiz Roberto Evangelista and Ervin Kaminski Lenzi. *Fractional diffusion equations and anomalous diffusion*. Cambridge University Press, 2018.

- [20] Duccio Fanelli and Alan J McKane. Diffusion in a crowded environment. *Physical Review E-Statistical, Nonlinear, and Soft Matter Physics*, 82(2):021113, 2010.
- [21] Ahmad Foroozani and Morteza Ebrahimi. Anomalous information diffusion in social networks: Twitter and digg. *Expert Systems with Applications*, 134:249–266, 2019.
- [22] Lazaros K Gallos, Chaoming Song, Shlomo Havlin, and Hernán A Makse. Scaling theory of transport in complex biological networks. *Proceedings of the National Academy of Sciences*, 104(19):7746–7751, 2007.
- [23] Sergio Gomez, Albert Diaz-Guilera, Jesus Gomez-Gardenes, Conrad J Perez-Vicente, Yamir Moreno, and Alex Arenas. Diffusion dynamics on multiplex networks. *Physical review letters*, 110(2):028701, 2013.
- [24] Rudolf Gorenflo, Anatoly A. Kilbas, Francesco Mainardi, and Sergei V. Rogosin. *Mittag-Leffler Functions, Related Topics and Applications*. Springer Monographs in Mathematics. Springer, Berlin, 2014.
- [25] Igor Goychuk. Viscoelastic subdiffusion in a random gaussian environment. *Phys. Chem. Chem. Phys.*, 20:24140–24155, 2018.
- [26] Igor Goychuk and Thorsten Pöschel. Fingerprints of viscoelastic subdiffusion in random environments: Revisiting some experimental data and their interpretations. *Physical Review E*, 104(3):034125, 2021.
- [27] Marco Grimaldo, Felix Roosen-Runge, Fajun Zhang, Frank Schreiber, and Tilo Seydel. Dynamics of proteins in solution. *Quarterly Reviews of Biophysics*, 52:e7, 2019.
- [28] Sudipta Gupta, Ralf Biehl, Clemens Sill, Jurgen Allgaier, Melissa Sharp, Michael Ohl, and Dieter Richter. Protein entrapment in polymeric mesh: Diffusion in crowded environment with fast process on short scales. *Macromolecules*, 49(5):1941–1949, 2016.
- [29] Morton E Gurtin and Allen C Pipkin. A general theory of heat conduction with finite wave speeds. *Archive for Rational Mechanics and Analysis*, 31(2):113–126, 1968.
- [30] Till Hoffmann, Mason A Porter, and Renaud Lambiotte. Random walks on stochastic temporal networks. In *Temporal Networks*, pages 295–313. Springer, 2013.
- [31] Conggui Huang and Fei Wang. Distributed consensus tracking of incommensurate heterogeneous fractional-order multi-agent systems based on vector lyapunov function method. *Fractal and Fractional*, 8(10):575, 2024.
- [32] Manisha Joshi, Savita Bhosale, and Vishwesh A Vyawahare. A survey of fractional calculus applications in artificial neural networks. *Artificial Intelligence Review*, 56(11):13897–13950, 2023.
- [33] Won Jung, Tai-Yen Chen, Ace George Santiago, and Peng Chen. Memory effects of transcription regulator- dna interactions in bacteria. *Proceedings of the National Academy of Sciences*, 121(41):e2407647121, 2024.
- [34] Eldad Kepten, Aleksander Weron, Grzegorz Sikora, Krzysztof Burnecki, and Yuval Garini. Guidelines for the fitting of anomalous diffusion mean square displacement graphs from single particle tracking experiments. *PLoS One*, 10(2):e0117722, 2015.
- [35] Hyunjoong Kim and Sean D Lawley. Cover times of many diffusive or subdiffusive searchers. *SIAM Journal on Applied Mathematics*, 84(2):602–620, 2024.
- [36] Mikko Kivelä, Alex Arenas, Marc Barthelemy, James P Gleeson, Yamir Moreno, and Mason A Porter. Multilayer networks. *Journal of complex networks*, 2(3):203–271, 2014.
- [37] T Kosztolowicz, K Dworecki, and St Mrózczynski. Measuring subdiffusion parameters. *Physical Review E-Statistical, Nonlinear, and Soft Matter Physics*, 71(4):041105, 2005.
- [38] Renaud Lambiotte, Vsevolod Salnikov, and Martin Rosvall. Effect of memory on the dynamics of random walks on networks. *Journal of complex networks*, 3(2):177–188, 2015.
- [39] Soonchih C Lim and Siti Vinayakam Muniandy. Self-similar gaussian processes for modeling anomalous diffusion. *Physical Review E*, 66(2):021114, 2002.
- [40] Li Lingfei, Zhou Xiuxiang, and Hang Gao. The stability and exponential stabilization of the heat equation with memory. *Journal of Mathematical Analysis and Applications*, 466(1):199–214, 2018.
- [41] Dunia López-Pintado. An overview of diffusion in complex networks. *Complex Networks and Dynamics: Social and Economic Interactions*, pages 27–48, 2016.
- [42] Jianquan Lu, Jun Shen, Jinde Cao, and Jürgen Kurths. Consensus of networked multi-agent systems with delays and fractional-order dynamics. In *Consensus and synchronization in complex networks*, pages 69–110. Springer, 2012.

- [43] Francesco Mainardi. *Fractional Calculus and Waves in Linear Viscoelasticity: An Introduction to Mathematical Models*. Imperial College Press, London, 2010.
- [44] Francesco Mainardi, Antonio Mura, and Gianni Pagnini. The m-wright function in time-fractional diffusion processes: A tutorial survey. *International Journal of Differential Equations*, 2010(1):104505, 2010.
- [45] Francesco Mainardi, Antonio Mura, and Gianni Pagnini. The m-wright function in time-fractional diffusion processes: a tutorial survey. arXiv preprint, 2010.
- [46] Steen Markvorsen. Minimal webs in riemannian manifolds. *Geometriae Dedicata*, 133(1):7–34, 2008.
- [47] Naoki Masuda, Mason A Porter, and Renaud Lambiotte. Random walks and diffusion on networks. *Physics reports*, 716:1–58, 2017.
- [48] Pablo Medina, Sebastián Carrasco, Paulina Correa-Burrows, José Rogan, and Juan Alejandro Valdivia. Nontrivial and anomalous transport on weighted complex networks. *Communications in Nonlinear Science and Numerical Simulation*, 114:106684, 2022.
- [49] Mark M. Meerschaert, Erkan Nane, and P. Vellaisamy. The fractional poisson process and the inverse stable subordinator. *Electronic Journal of Probability*, 16:1600–1620, 2011.
- [50] Mark M. Meerschaert and Alla Sikorskii. *Stochastic Models for Fractional Calculus*, volume 43 of *De Gruyter Studies in Mathematics*. de Gruyter, Berlin, 2011.
- [51] Lina Meinecke. Multiscale modeling of diffusion in a crowded environment. *Bulletin of mathematical biology*, 79(11):2672–2695, 2017.
- [52] Ralf Metzler and Joseph Klafter. The random walk’s guide to anomalous diffusion: a fractional dynamics approach. *Physics reports*, 339(1):1–77, 2000.
- [53] Christos Nicolaides, Luis Cueto-Felgueroso, and Ruben Juanes. Anomalous physical transport in complex networks. *Physical Review E–Statistical, Nonlinear, and Soft Matter Physics*, 82(5):055101, 2010.
- [54] Zaid Odibat. Approximations of fractional integrals and caputo fractional derivatives. *Applied Mathematics and Computation*, 178(2):527–533, 2006.
- [55] Guofei Pang, Lu Lu, and George Em Karniadakis. fPINNs: Fractional physics-informed neural networks. *SIAM Journal on Scientific Computing*, 41(4):A2603–A2626, 2019.
- [56] Piotr Polanowski and Andrzej Sikorski. Simulation of diffusion in a crowded environment. *Soft Matter*, 10(20):3597–3607, 2014.
- [57] Rodrigo Ponce. Discrete subdiffusion equations with memory. *Appl. Math. Optim.*, 84(3):3475–3497, December 2021.
- [58] Summaya Saif and Salman Malik. An inverse problem for a two-dimensional diffusion equation with arbitrary memory kernel. *Mathematical Methods in the Applied Sciences*, 46(9):11007–11020, 2023.
- [59] Trifce Sandev, Zivorad Tomovski, Johan LA Dubbeldam, and Aleksei Chechkin. Generalized diffusion-wave equation with memory kernel. *Journal of Physics A: Mathematical and Theoretical*, 52(1):015201, 2018.
- [60] Michael J Saxton. Anomalous subdiffusion in fluorescence photobleaching recovery: a monte carlo study. *Biophysical journal*, 81(4):2226–2240, 2001.
- [61] René L. Schilling, Renming Song, and Zoran Vondraček. *Bernstein Functions: Theory and Applications*, volume 37 of *De Gruyter Studies in Mathematics*. de Gruyter, Berlin, 2 edition, 2012.
- [62] Ingo Scholtes, Nicolas Wider, René Pfitzner, Antonios Garas, Claudio J Tessone, and Frank Schweitzer. Causality-driven slow-down and speed-up of diffusion in non-markovian temporal networks. *Nature communications*, 5(1):5024, 2014.
- [63] Grant Silver, Meisam Akbarzadeh, and Ernesto Estrada. Tuned communicability metrics in networks. the case of alternative routes for urban traffic. *Chaos, Solitons & Fractals*, 116:402–413, 2018.
- [64] Igor M Sokolov. Models of anomalous diffusion in crowded environments. *Soft Matter*, 8(35):9043–9052, 2012.
- [65] Igor M Sokolov, Joseph Klafter, and Alexander Blumen. Fractional kinetics. *Physics Today*, 55(11):48–54, 2002.
- [66] Fenglan Sun, Yunpeng Han, Wei Zhu, and Jürgen Kurths. Group consensus for fractional-order heterogeneous multi-agent systems under cooperation-competition networks with time delays. *Communications in Nonlinear Science and Numerical Simulation*, 133:107951, 2024.

- [67] Wei Sun, Yan Li, Changpin Li, and YangQuan Chen. Convergence speed of a fractional order consensus algorithm over undirected scale-free networks. *Asian Journal of Control*, 13(6):936–946, 2011.
- [68] Nguyen Duong Toan et al. The nonclassical diffusion equations with time-dependent memory kernels and a new class of nonlinearities. *Glasgow Mathematical Journal*, 64(3):716–733, 2022.
- [69] Lloyd N. Trefethen and J. A. C. Weideman. The exponentially convergent trapezoidal rule. *SIAM Review*, 56(3):385–458, 2014.
- [70] Steffen Trimper, Knud Zabrocki, and Michael Schulz. Memory-controlled diffusion. *Physical Review E–Statistical, Nonlinear, and Soft Matter Physics*, 70(5):056133, 2004.
- [71] Matthias Weiss, Markus Elsner, Fredrik Kartberg, and Tommy Nilsson. Anomalous subdiffusion is a measure for cytoplasmic crowding in living cells. *Biophysical journal*, 87(5):3518–3524, 2004.
- [72] Xu Yan, Kun Li, Chengdong Yang, Jiaojiao Zhuang, and Jinde Cao. Consensus of fractional-order multi-agent systems via observer-based boundary control. *IEEE Transactions on Network Science and Engineering*, 11(4):3370–3382, 2024.

SCUOLA NORMALE SUPERIORE, PISA, ITALY. E-MAIL: NIKITA.DENISKIN@SNS.IT; INSTITUTE FOR CROSS-DISCIPLINARY PHYSICS AND COMPLEX SYSTEMS (IFISC), CSIC-UIB, PALMA DE MALLORCA, SPAIN. E-MAIL: ESTRADA@IFISC.UIB-CSIC.ES